Center for Advanced Bio-Based Binders and Pollution Reduction Technologies

Award Number: DE-FG36-06G086029

Recipient: University of Northern Iowa, 1222 West 27th Street, Cedar Falls. IA 50614-0178
Project Location: University of Northern Iowa, 1222 West 27th Street, Cedar Falls. IA 50614-0178

Project Period: July 1, 2005 through June 30, 2009
Date of Report: 09/30/2009
Written by: Jerry Thiel
Program Manager: Edward Ebert
Principle Investigators: Jerry Thiel

Subcontractors: Christoph Beckermann - University of Iowa, Fred Cannon – Penn State University, William Tordoff - American Metalcasting Services International, Inc., Joan Combie – Montana Polysaccharides

Cost-Sharing Partners: University of Northern Iowa

Project Contact(s): Jerry Thiel, 319-273-7085, thiel@uni.edu

Document Availability: Reports are available free via the U.S. Department of Energy (DOE) Information Bridge:

Web Site http://www.osti.gov/bridge

Reports are available to DOE employees, DOE contractors, Energy Technology Data Exchange (ETDE) representatives, and Informational Nuclear Information System (INIS) representatives from the following source:

Office of Scientific and Technical Information
P.O. Box 62
Oak Ridge, TN 37831
Tel: (865) 576-8401
Fax: (865) 576-5728
E-mail: reports@osti.gov
Web Site: http://www.osti.gov/contact.html

Acknowledgment: This material is based upon work supported by the Department of Energy under Award Number DE-FG36-06G086029

Disclaimer: This report was prepared as an account of work sponsored by an agency of the United States Government. Neither the United States Government nor any agency thereof, nor any of their employees, makes any warranty, express or implied, or assumes any legal liability or responsibility for the accuracy, completeness, or usefulness of any information, apparatus, product, or process disclosed, or represents that its use would not infringe privately owned rights. Reference herein to any specific commercial product, process, or service by trade name, trademark, manufacturer, or otherwise does not necessarily constitute or imply its endorsement, recommendation, or favoring by the United States Government or any agency thereof. The views and opinions of authors expressed herein do not necessarily state or reflect those of the United States Government or any agency thereof.

Table of Contents

Section	Page
List of tables and figures	5
Executive summary	8
Introduction	9
Background	10
Project team members	11
Research and Development	13
Section 1 Saccharides and Lignite replacements	14
Saccharides	
Lignite	15
Biobased isocyanates	16
Accomplishments	17
Conclusions	17
Section 2 Fermented saccharides (Levan)	18
Test Procedures	18
Results and Discussion	18
Solvent for Levan	18
Chemical curing	19
Emulsifiable MDI	19
Cross-linking Levan with MDI	19
Catalyst – DABCO & DBTA	20
Catalyst –Jeffcat DMDEE	20
Chemical Curing – Melamine and Titanate	24
Levan without additives	25
Accomplishments	27
Recommendations	27
Section 3 Mathematical mold gas emission modeling	
Project Executive Summary	28
Introduction	30
Mold/Core gas model	31
Gaseous species conservation	32
Gas velocity	32
Gas pressure equation	32
Energy equation	33
Condensation/vaporization model	33
Pyrolysis model	34

Section	Page
Measured pyrolysis data	35
TGA pyrolysis emission analysis for total amounts of pyrolysis products	35
TGA pyrolysis-mass spectrometer (MS) analysis for continuous pyrolysis analysis	36
Pyrolysis results and correlation	37
Development of pyrolysis model parameters	37
Mold/core gas simulation examples	39
One dimensional sand sample simulation	39
Tree core simulation	40
Validation casting experiments	41
Validation methodology and results	41
Model deviation from casting experiment	42
Casting verification conclusions/recommendations	44

Lists of Figures, Tables and Appendices

Section 2

Figure 1: Ratios of catalysts tested with levan-MDI formulations. 19

Figure 2: In the manual mixing system, typical formulations shown resulted in reasonable work and strip times, but the scratch hardness did not reach suitable levels as quickly as required for a high through put system 20

Figure 3: Order of addition for levan, MDI and DMDEE catalyst. 21

Figure 4: Use of levan coated sand to slow reaction rate. 21

Figure 5: 25% levan-water-alcohol and 75% emulsifiable MDI binder was used at a rate of 2% 22

Figure 6: This table shows the effect of activation temperature and time on cross-linking with PAE. 23

Figure 7*:* 225 F for 1 hr resulted in cores of moderate hardness for samples bonded with levan in a water-alcohol solution but with no other additives. 24

Figure 8: Use of levan/water/ethanol as binder with no other additions. The binder was held at 113 or 122 F 25

Figure 9: Heating sand cores bonded by levan in water/ethanol at 250 F for only 10 min, resulted in samples that had already reached strip time upon removal from the oven and maximum scratch hardness at only 1 hr. 25

Section 3

Table 1. Total amounts of pyrolysis products captured during TGA pyrolysis of the first sample from 20°C – 900°C at 10°C/min. 44

Figure 1. Total binder mass and pyrolysis rate of the second sample as functions of temperature. Values given as a percent of the original binder mass (%OBM). 44

Figure 2. Captured greenhouse gas pyrolysis products from the first sample as a function of temperature range. 45

Figure 3. Kinetic measurements of individual gaseous species from pyrolysis of the second sample. 46

Figure 4. (a) Mass spectrometer (MS) data for benzene, given as normalized current, and the integral of the area under the normalized current curve; (b) Production rate of benzene and total mass of benzene generated, given as a mass fraction. 47

Figure 5. (a) Two model peaks fit to peaks in benzene production rate data; and (b) sum of model peaks, compared to benzene production rate curve. 48

Figure 6. Comparison of total binder mass lost and mass lost due to the 11 species listed in Table 1, as well as a comparison of the corresponding pyrolysis rates. 49

Figure 7. Total pyrolysis products generated, pyrolysis products generated due to the 11 species in Table 1, and the 'other' pyrolysis products generated. 49

Figure 8. Binder mass lost due to pyrolysis products not listed in Table 1, along with the production rate of these 'other' pyrolysis products. 50

Figure 9. Production rate of 'other' pyrolysis products, along with modeled production rate. 50

Figure 10. Comparison between (a) measured and modeled total pyrolysis rates; and (b) measured and modeled binder mass, as functions of temperature. 51

Figure 11. Schematic of domain for 1-D example. 52

Figure 12. Temperature profiles at various times during the simulation. 52

Figure 13. Binder mass concentration profiles at various times during the simulation. 53

Figure 14. Cresol pore volume fraction profiles at various times during the simulation. 53

Figure 15. Liquid cresol concentration profiles at various times during the simulation. 54

Figure 16. Binder mass and pyrolysis rate as a function of time for sand sample. 54

Figure 17. Cumulative species emissions that reach the outlet as a function of time: (a) mass scale showing largest components; and (b) mass scale showing smaller components. 55

Figure 18. Schematics of tree core: (a) top view; and (b) side view. 56

Figure 19. Tree core temperature profiles at various times during the simulation. 56

Figure 20. Tree core pressure profiles at various times during the simulation. 57

Figure 21. Tree core binder mass concentration profiles at various times during the simulation. 58

Figure 22. Tree core pressure profiles at various times during the simulation. 58

Table 2. Emission Production of Model Validation Experiments 59

Table 3. Comparison of Ratio of HAP's produced during Validation Casting Experiment and Analytical Measurement. 59

Executive Summary

The Center for Advanced Biobased binders was formed to work closely with the US manufacturing industry to develop biobased replacements for oil based materials considered to have negative impact on both human health and the environment. The center was housed within the Metal casting Center at the University of Northern Iowa. The center is nationally recognized as a leader in cast metals research and has achieved unique stature as the premiere not-for-profit US research and training facility specializing in manufacturing technologies and environmental compliance for the foundry industry. The center's primary mission is to assist the foundry industry by developing technical solutions to this primary industry competitive in a global economy. The MCC is supported by a network of outreach and research centers at the university. These include the National Ag-Based Industrial Lubricants laboratory (NABL) and the Iowa Waste Reduction Center (IWRC), and state, regional, and national foundry business partners. The MCC testing laboratory and pilot-plant demonstration facility are the most advanced of their kind.

The project focus included building the Center's infrastructure that was necessary to provide industry focus and direction to the research. This industry focus will assure that technologies created during the research are what the industry needs and what they will be prepared to adopt in the future. The infrastructure consist primarily of the formation of the CABB staff, definition of the management structure and the development of sub recipient relationships and cost share arrangements with industry and other research organizations. Research conducted within the scope of the project included basic research and development work towards advanced bio-based binders and foundry pollution reduction.

The project was organized in four distinct phases. The first three of the phases included organization efforts including staffing of the center along with equipment purchases and the development of university – industry collaborations. The fourth and largest phase of the project included two major areas of research and development including substitution of petrochemical derivatives with biobased or natural materials and the development of simulation methodology to determine the beneficial effects of the substitutions. The forth phase devoted to research and development efforts is separated into three functional areas. These areas include phenol and formaldehyde substitutions in phenolic urethane polymers using saccharides and naturally occurring lignite materials, phenol and formaldehyde substitutions in phenolic urethane polymers using saccharides derived from fermentation of sugar beets, and the mathematical modeling of decomposition products relating to the use of phenolic urethane sand binders.

The project concentrated on developing possible strategies for substituting biobased and agricultural materials for those that are produced from petrochemical (crude oil) based materials. The scope of the project was limited to polymers used in the bonding of refractory materials used in the metal casting process. The cost of these petrochemical materials is highly dependent on political issues and the cost of crude oil. Recent tests to determine decomposition products of these petrochemical products show a strong correlation to the amount of hazardous air pollutants (HAP's) that are emitted as metal castings are produced.

The research was very successful in developing two possible substitutions for phenol and formaldehyde (PF) used in phenolic urethanes for foundry binders. Saccharides in the form of

commercial corn syrup was successfully substituted for PF showing comparable if not increased performance. Lignite, a naturally occurring organic material was also used successfully used as a substitute for PF in urethane foundry binders. These substitutions have the advantage of replacing a petroleum based material with both renewable and naturally occurring materials that are environmentally friendly, cost effective and plentiful. International patents were applied for on November, 14th 2009 and were issued WO 2009/65018 A1 and WO 2009/65015 A1. Current negotiations are underway with an industry supplier to commercialize and market the materials developed within the scope of the project.

Recommendations for future research include the continuation and broadening of the scope of the research to include commercial polymers used to manufacture plastic parts for various components. Future research would also include heat setting polymers as well as conventional urethane polymers providing the widest applicability to the industry.

Introduction

The project focused on the technology involved in metal casting, specifically in the polymeric sand binder systems. Molten metal is poured into molds made of sand to form the outer shape of the metal object, and cores of sand are used to create hollow areas in the metal object. Prior to the actual metal casting, the polymeric binder system is mixed with the sand and hardened to hold the sand in the desired shape. The molds and cores that are formed are single-use objects, since the binder "burns out" during the metal casting. The sand is recycled several times into new molds and cores, but the binder cannot be recycled. A foundry produces and uses hundreds of molds and cores each day. Even though the binder is typically added at only 0.5-2% of the weight of the sand, the worldwide foundry industry consumes 1 billion pounds of binder each year.

The foundry binder that currently accounts for 80% of the binder use is the amine-cured phenolic urethane system. The desirable characteristics of this binder are its short reaction time, the lack of volume change on curing, the hardness of the cured molded sand objects, and the breakdown of the binder at high temperature so that the sand can be shaken out of hollows in the casting. The undesirable characteristics of the amine-cured phenolic urethane system are the use of increasingly-expensive and non-renewable petroleum-based main components and solvents, the volatile organic compounds (VOCs) emitted during its curing and during casting, the odor, the emission of benzene, phenol, and a host of other carcinogens during casting, and poor shake-out performance in lower temperature casting applications such as aluminum casting. Our goal was to find environmentally-friendly cost-effective bio-based replacements for the two main components of the phenolic urethane binder. In order for our replacements to be acceptable to the foundry industry, we needed to maintain or improve upon the desirable characteristics, while minimizing the undesirable characteristics. In addition, any replacement needed to work with existing foundry mixers and pumping systems for the binder and sand.

In addition to the foundry industry, phenolic urethanes (and other polyurethanes) are used in many other applications, ranging from coatings to foam insulation to medical plastics. Therefore, the potential impact of our project is much larger than the foundry industry alone. The main benefits gained from our project are reducing U.S. dependence on petroleum,

improved environmental characteristics and emissions, improved worker environment (low odor), good shake-out performance, and use of abundant and/or renewable resources. At the foundry-use level, there will be an energy savings as a result of our project due to the shake-out performance, since less energy will be needed for sand reclamation/recycling.

Commercialization efforts of the technologies developed are ongoing through the end of the project period. Several companies have expressed interest in the intellectual property and currently evaluating the possibility of marketing and distribution of consumer products based on the technology. It is expected that commercialization of products based on the technologies developed during the project will begin early in 2010.

Background

In order to make cast iron or cast aluminum objects such as engine blocks, valves, agricultural machinery, etc., molten metal is poured into a mold and allowed to cool until it hardens and retains the shape of the mold. Not many substances can withstand the heat of molten iron, but the ancients knew that sand could, and sand is still used today to make the molds (which shape the outer surfaces of a cast metal object) and cores (which fill the hollow areas of a cast metal object). To hold the sand in the desired shape, a polymeric binder is mixed with the sand before it is formed into the molds and cores. The binder hardens as it cures. The most widely used foundry binder system today is phenolic urethane. This system consists of three parts. Part I is the phenolic resin, generally a phenol-formaldehyde polymer. Part II is the isocyanate resin, most often a combination of methylene diphenyl diisocyanate (MDI) and polymeric forms of MDI. Part III, a small percentage of the total binder weight, is the tertiary amine catalyst, which may be dissolved in solvent and mixed with Parts I and II (no-bake or air-set method) or may be injected as a gas or aerosol into the molded sand object (cold-box method).

The phenolic urethane binder is quite successful in several regards. It hardens (cures) very rapidly, in seconds using the cold box method, or in minutes using the no-bake method. It has sufficient hardness and tensile strength to permit the cured molds and cores to be moved from place to place, and some of them are large enough to require a fork truck. There is no volume change during curing, so the dimensions of the finished cast metal object can be predicted easily. And it burns out during the cooling of the molten metal, so that the cores can be shaken out of the hollow areas and the sand can be recycled several times. The disadvantages of the phenolic urethane are its odor; the toxicity/carcinogenicity of the components (phenol, formaldehyde, MDI, aromatic solvents, tertiary amines); the emission of a host of VOCs and other air pollutants during mixing, curing, casting, and shake out; and the petroleum origin of all the components, which increases U.S. dependence on foreign oil and costs significantly more now than it did in the 1960s when the phenolic urethane system was introduced in the foundry industry.

Our project goal was to find environmentally-friendly, cost-effective, bio-based replacements for the two main components of the phenolic urethane binder system, Part I and Part II. We were mainly attempting to find non-petroleum-based replacements, to alleviate the rising cost of conventional binder and reduce U.S. dependence on foreign oil. Bio-based replacements have the advantage of being a renewable resource, and it was our additional objective to

improve the emission characteristics of the binder system overall. In order to be acceptable to the foundry industry, any replacement needs to approximately meet or exceed current binder performance in the desired characteristics of reaction time, physical properties (hardness and tensile strength), lack of volume change, and burn-out/shake-out. In addition, a replacement must be compatible with current foundry binder/sand mixing and pumping technology, which necessitates a certain viscosity for the binder. Finally, the casting performance (as measured by veining, bubbles, surface finish, etc. in the cast metal object) of the binder system that uses a replacement must be comparable to or better than phenolic urethane. It was an ambitious goal to find replacements that met all these criteria. Since the isocyanate resin (Part II) will react with many types of compounds, we focused first on replacements for Part I. As those replacements were identified and moved into the formulation stage, we turned out attention to finding a Part II replacement, a more difficult prospect. Since isocyanates are so reactive, they do not exist in nature, so our focus was on synthesizing a di-isocyanate from a bio-based source.

Project Team Members:

Jerry Thiel is the Director of the Metal Casting Center at the University of Northern Iowa. He has a diverse industrial background and has held management positions in the metal casting and related industries for over 30 years. His background includes metal casting experience in steel, iron and non-ferrous alloys. Mr. Thiel holds degrees in materials science, manufacturing and manufacturing process development and has published numerous research papers pertaining to molding and core materials for the foundry industry. He is a past chairman of the Hawkeye chapter of the American Foundry Society as well as currently serving on the AFS 4A, 4B, 4N, 4K and 4H national committees.

Shoshanna Coon (B.S. Chemistry, Indiana University, Bloomington, IN; Ph.D. Physical Chemistry, University of Texas, Austin, TX; Postdoctoral work, University of Iowa, Iowa City, IA) is an Associate Professor of Chemistry at University of Northern Iowa. Although her research is primarily in surface chemistry, she had some prior background in polymer chemistry. Working with several undergraduate and graduate research assistants, her project goals were to identify replacements for Part I and Part II of the phenolic urethane foundry binder.

Scott R. Giese, associate professor at the University of Northern Iowa (UNI), is the FEF Key Professor for the metal casting program at the university. Originally from Buffalo, NY, Dr. Giese is a second generation foundry person. A dual associate degree graduate of Erie Community College in Material Science and Engineering Science, he transferred to the University of Alabama and received his B.S., M.S., and Ph.D in Metallurgical Engineering. Upon graduation, he was employed at the UNI Metal Casting Center as a research project manager for eight years managing applied research projects and conducting training program for the metal casting industry. For the last six years, he has taught in the manufacturing technology program as a tenure faculty member in the UNI Department of Industrial Technology. He has authored over 20 papers and presented 50 technical discussions on casting solidification and foundry technologies.

Beckermann, Christoph: Is currently a University of Iowa Foundation Distinguished Professor of Mechanical and Industrial Engineering at The University of Iowa. He received M.S. and Ph.D. degrees in Mechanical Engineering at Purdue University. He received a National Science Foundation Presidential Young Investigator Award. He is the author/co-author of about 100 refereed journal articles and 90 papers in conference proceedings. Dr Beckermann directs the Solidification Laboratory. Dr. Beckermann also serves on the editorial board of several journals and has organized numerous symposia and conferences. He is a Fellow of the American Society of Mechanical Engineering (ASME) and a member of TMS, ASM, MRS, AIAA, and ASEE.

Fred Cannon: Is currently a full professor at the Pennsylvania State University. He Received his Ph.D. Degree in Environmental Engineering at the University of Illinois, Champaign-Urbana, his M.S. And Degree of Advanced Engineer in Environmental Engineering at Stanford University, and his Bachelors in Civil Engineering at University of California Davis. He has received NSF funding for 15 consecutive years. He is author / co-author of about 60 refereed journal articles. Dr. Cannon conducts research in Environmental Engineering pertaining to porous carbon materials for the environment. He is a member of American Water Works Association, American Carbon Society, and is active in the American Foundry Society. He is on the advisory committee of the ACS.

Joan Combi: Is the President of Montana Polysaccharides Corp. (MPC), a research and development company focusing on the use of microorganisms as a source of natural products and environmentally friendly processes. Combie received her Ph.D. in 1982 and founded the predecessor of MPC in 1986.

James Yavorsky: Has over 20 years of experience applying polymer science, surface science and engineering to develop unique and valuable products from concept through customer introduction. His proven strengths include problem definition, laboratory scale characterization, small scale and pilot scale test method development and scale up processing. Jim has have been instrumental in bringing experimental products to industrial scale, acting as liaison with marketing and technical service to introduce products through presentations, publications and trade shows as well as dealing with regulatory issues, codes and intellectual property issues.

Research and Development Efforts

Section 1 - Substitution of phenol, formaldehyde and aromatic solvents with corn based polysaccharides and naturally occurring humic acid containing lignite.

Conventional phenolic urethane foundry binder is a three-part system. Part I is the phenol-formaldehyde resin, which contains about 50% aromatic solvents and other components. Part II is the isocyanate resin, which also contains about 50% aromatic solvents/other components. These two parts together account for approximately 90% of the weight of the binder. Part III is the catalyst component, which contains a tertiary amine. In the no-bake method, liquid Part III is added to Part I prior to mixing with Part II and sand and packing the sand into molds. The treated sand cures and hardens within the mold until it is firm enough to be removed. In the cold-box method, after Part I, II and sand are mixed and the bound sand is packed into a mold, the Part III is injected as a gas or aerosol into the sand, curing the treated sand in a very short time. Although the cold-box method allows for very short cure times, it requires specialized molds for gassing the molded sand and also gas handling equipment for reclaiming the amine catalyst. For this reason, many foundry applications still use the no-bake method, and reaction time is a chief consideration of the binder system in that method.

We chose to utilize the urethane cross-linking chemistry that gives the phenolic urethane system some of its most desirable properties, such as lack of volume change during reaction, rather than to attempt to discover new polymer chemistry entirely. Our project goal was then to identify replacements for both Part I and Part II of the conventional phenolic urethane binder. In the ideal case, the replacements will be low-cost, environmentally-friendly, bio-based, renewable resource materials that can be formulated to meet or exceed conventional binder performance. As described below, we succeeded in achieving these characteristics with the Part I replacement. The Part II replacement proved to be more challenging.

<u>Part I Replacements</u>

I) Saccharides

The isocyanate functionality of Part II will react with many types of compounds, but to simplify our search for replacements for phenol-formaldehyde (Part I), we focused on hydroxyl-containing bio-based compounds. Our assumption was that they would mimic the hydroxyl functionality of the phenol-formaldehyde. We started our investigation with pullulan, a polymer of glucose. Although pullulan did not dissolve in the conventional Part I solvents, it first showed promise as a filler material, and later as a complete replacement for Part I. The barriers to its use in a foundry setting were its high cost and its hydrophilic nature, which necessitated using water as part of the solvent package. Water is detrimental to urethane polymer formation because water consumes the isocyanate, and the desired urethane linkages are susceptible to hydrolysis. In addition, water is incompatible with the solvent packages used in the Part II (isocyanate) and Part III (tertiary amine catalyst) components.

Since the main problem with pullulan was its large molecular weight and hydrophilicity, we tried smaller saccharides, which also contain the hydroxyl functionality. We found that

sucrose, corn syrup, high fructose corn syrup and molasses all made a polymer with conventional Part II isocyanates. The best results were obtained with corn syrup, and formulation efforts focused on increasing the compatibility with existing foundry machinery and processes by adjusting the viscosity and optimizing reaction speed and physical properties. We succeeded in formulating a saccharide-based Part I replacement that can be directly substituted for conventional Part I in foundry applications, and it meets or exceeds the needs of the foundry industry in physical properties and casting performance. Field trials at local foundries in the final quarter of the project demonstrated that a binder using our saccharide based Part I replacement could withstand the high temperature conditions of both stainless steel and gray iron casting. In the trials, the surface finish was as good or better than the finish with the binder system currently used by the foundry. In addition, the saccharide-based binder burned away more completely for easier shake-out, indicating a significant energy and cost savings in the shake-out and sand reclamation/recycling process. Compared to the conventional binder, a definite improvement in odor and irritating emissions from mixing through shake-out was noted by the foundry employees.

II) Lignite

Lignite is "brown coal", the lowest rank of coal. It is a cheap, abundant U.S. natural resource, currently used mainly for electric power generation due to its low heat value. Lignite contains many different functionalities—including hydroxyl groups, carboxylic acid groups, and amine groups—that can react with the isocyanate functionality of Part II. In exploring the possibility of using lignite as a Part I replacement, the problem of solubility or suspendability was the most challenging to address. At least 10 different solvents were tested, with success as a binder in many cases. However, the shelf life of the replacement resin was limited. Balancing viscosity and suspension stability became the key to commercialization. By a combination of solvent choice and high shear mechanical processing, we were successful in preparing a suspension that is stable for approximately a month and compatible with existing foundry machinery.

Field trials at local foundries in the final quarter of the project demonstrated that a binder using our lignite-based Part I replacement could withstand the high temperature conditions of both stainless steel and gray iron casting, in both no-bake (liquid catalyst) and cold-box (gaseous catalyst) processes. In the trials, the surface finish was as good or better than the finish with the binder system currently used by the foundry. In addition, the lignite-based binder burned away more completely for easier shake-out, indicating a significant energy and cost savings in the shake-out and sand reclamation/recycling process. The odor and irritating emissions were noticeably less compared to the conventional binder.

<u>Part II Replacement</u>

Part II of the conventional phenolic urethane binder system is an isocyanate resin, typically containing Methylene diphenyl diisocyanate (MDI) and polymeric MDI and solvents/additives. The important functionality is two isocyanate groups per molecule (diisocyanate), allowing polymerization along with cross-linking to the hydroxyl-containing Part I. The typical formulation of a conventional Part II is 50% isocyanate and 50% aromatic solvents and other components. Since the isocyanate functionality is very reactive with many other

functionalities, there are no naturally occurring isocyanates to isolate as a potential replacement. Therefore, our efforts focused on using organic chemistry synthesis techniques to convert a bio-based feedstock into a diisocyanate. The work on this synthesis took place in parallel with much of the formulation work on the Part I replacements, with some personnel devoted to the synthesis and others devoted to the Part I.

The most direct synthetic route to a diisocyanate is to perform phosgenation on a diamine. Phosgenation is used commercially to produce MDI from petroleum feedstocks, but due to the hazards of phosgene and the need to exclude moisture from the reaction, only one or two companies do all the phosgenation in the United States. We determined that we could safely, but at considerable expense, perform a small scale phosgenation using diphosgene, a liquid, so our initial strategy was to identify bio-based diamines to phosgenate into diisocyanates. By consulting a biochemist at our university, we found that living systems produce only two diamines naturally: putrescine (tetramethylene diamine) and cadaverine (pentamethylene diamine). As their names suggest, these compounds are produced by decaying animal flesh, and are partially responsible for its foul smell. We purchased putrescine from a chemical company and were able to successfully phosgenate it to tetramethylene diisocyanate, as demonstrated by the characteristic peak for isocyanate at 2273 cm^{-1} in infrared spectroscopy and the lack of amine peaks in the spectrum. However, the compound was not stable under our conditions, so we were unable to isolate enough to test with Part I to determine if it would make a polymer. However, we had proved that we could convert an aliphatic diamine to a diisocyanate.

Because of the expense and hazards of phosgenation, we attempted a different synthetic route from the diamine to the diisocyanate, using Mitsunobu chemistry and carbon dioxide in methylene chloride at very low temperature, which had been shown to produced good yields of isocyanate from aryl and hindered alkyl amines.[1] The reaction was challenging technically and also proved to be difficult to extend to the diamine to create a diisocyanate. Therefore, we continued to use phosgenation to convert diamines to diisocyanates.

Since there is no abundant biological source of diamines, we next implemented a strategy of starting with an abundant, renewable bio-feedstock and creating a diamine from that in several synthesis steps. We worked out on paper a reaction scheme to convert vegetable oils to heptamethlene diamine. The basic steps of our original scheme were

1. Saponification of vegetable oil to produce the free fatty acids.
2. Oxidation of the free fatty acids to produce azelaic acid (1,9-nonanedioic acid).
3. Conversion of azelaic acid to heptamethylene diamine using the Schmidt reaction.
4. Phosgenation of heptamethylene diamine to heptamethylene diisocyanate.

Steps 1, 2, and 4 were successfully accomplished on small scale. We did a study of saponification conditions and successfully produced free fatty acids, but later found that the most economically viable source of free fatty acids is likely to be the biodiesel industry. Free fatty acids are an unwanted byproduct in the production of biodiesel. We studied three different means of oxidation: metavanadate oxidation, permanganate oxidation, and ozonolysis. The metavanadate oxidation was abandoned as being too expensive to use commercially. Permanganate oxidation worked well, but isolation of the product was a

challenge due to the manganese dioxide product present in suspension. Ozonolysis was found to be the best choice for oxidation, since it produces the product in a mixture that can be separated relatively easily. After repeated attempts at the Schmidt reaction with little product, and an explosion in a hood, the Schmidt reaction was abandoned as being unsafe and ineffective on aliphatic diacids. Since we were unable to complete Step 3, we proceeded to step 4 using purchased heptamethlyene diamine. We were successful in phosgenating it to create heptamethylene diisocyanate at 66% yield. We tested it with conventional Part I resin and performed thermal analysis (Differential Scanning Calorimetry, DSC, and Thermal Gravimetic Analysis, TGA) on the resulting polymer. The polymer that formed was more flexible than conventional phenolic urethane, which is not surprising given that our isocyanate is not as rigid a molecule as MDI. The DSC and TGA results showed that the polymer made with heptamethylene diisocyanate decomposed at a lower temperature than conventional phenolic urethane. However, this does not preclude its use in the foundry industry or in other applications. Indeed, a similar isocyanate, hexamethylene diisocyanate (HDI), is used extensively in medical polyurethane applications.

To avoid using the Schmidt reaction, we devised several new reaction schemes starting from the end of Step 2. These were the following:

- Scheme A was to convert azelaic acid to the diamide and then use a Hoffman rearrangement to convert the diamide to the diamine and then the diamine is phosgenated to give heptamethylene diamine.
- Scheme B was to also convert azelaic acid to the diamide, but then the diamide is reduced with lithium aluminum hydride to give nonamethylene diamine, which is then phosgenated to give nonamethylene diisocyanate.
- Scheme C was to reduce azelaic acid to 1,9-nonanediol with lithium aluminum hydride, then to replace the hydroxyl groups of the diol with bromine to give 1,9-dibromononane, then to react the dibromo compound with potassium cyanate or silver cyanate, one of which should give nonamethylene diisocyanate.

The initial step of Scheme A was accomplished successfully, but we were unable to make any diamine product using the Hoffman rearrangement before the end of the project. Schemes B and C both involved a reduction with lithium aluminum hydride (LAH), which bursts into flames if it contacts water. We attempted the LAH reduction in Scheme C, but it appeared that no diol product was produced. Due to the hazards of this reaction, we did not pursue Schemes B or C.

Accomplishments

Part I Replacements: We developed two binder systems, based on bio-based Part I replacements, that are compatible with existing foundry machinery. Both binders feature lower levels of VOCs, lower levels of hazardous air pollutants, and lower odor. They were successfully field tested and met or exceeded foundry specifications, notably with better surface finish and better shake-out than conventional binders. The shake-out characteristics in particular translate into direct energy savings in the sand reclamation/recycling step of foundry operations.

Two patent applications have been filed, and both binder systems have been licensed to a foundry binder supplier.

Part II Replacements: We identified and successfully produced two diisocyanates, tetramethylene diisocyanate and heptamethylene diisocyanate, that could have bio-based sources, although we used purchased chemicals as starting materials. Heptamethylene diisocyanate was produced in sufficient quantity for preliminary testing of its reactivity with conventional Part I and of the properties of the resulting polymer. Near the end of the project, another researcher published a synthesis of our main target compound, heptamethylene diisocyanate, from vegetable oil, using a different route from azelaic acid to the diisocyanate. [2] This shows that our main idea was sound, although our synthetic route was not ultimately successfully. We are discussing a possible collaboration with this researcher.

Conclusions

The project was very successful in determining biobased and naturally occurring substitutions for petrochemical derived materials used for the boning of sand used in the metal casting process. Simple corn syrup along with lignite were two materials that have been found to be very effective in replacing both phenol and formaldehyde in the manufacture of phenolic urethane polymer adhesives. These materials have the ability to reduce dependence on foreign oil while reducing the hazardous emissions associated with phenol, formaldehyde and volatile organic compounds (VOC's). Current negotiations are underway with an industry supplier to commercialize and market the materials developed within the scope of the project.

References / Bibliography

[1] Horvath, M. J.; Saylik, D.; Elmes, P. S.; Jackson, W. R.; Lovel, C. G.; Moody, K. *Tetrahedron Lett.* **1999**, *40*, 363.

[2] Hojabri, Leila; Kong, Xiaohua; Narine, Suresh S. *Biomacromolecules* **2009** *10*, 884.

Section 2 - Substitution of phenol, formaldehyde and aromatic solvents with fermentation based polysaccharides.

TECHNICAL APPROACH AND HYPOTHESIS:

Sand core binders used in foundry applications often include toxic chemicals such as formaldehyde. Bio-based materials are a potential option for more environmentally friendly binders. Levan, a polysaccharide with known adhesive properties, was selected for testing as a foundry binder during this project.

Levan is biodegradable and non-toxic even when incinerated. This fructan polymer has an extremely low intrinsic viscosity. Unlike most biopolymers, levan forms spheres which contribute little to solution viscosity. The good flowability makes formulations easier to handle and decreases the amount of energy required for mixing.

TEST PROCEDURES:

Initially, samples were prepared and qualitatively evaluated. As more suitable formulations were developed, scratch hardness tests and green hardness (work and strip times) were determined on 50 gm samples. Later tests done at the Metal Casting Center also included preparation of dog bones for tensile strength measurement.

To ascertain the hardness of the sand core surface, a four point spring loaded cutter from Simpson-Gerosa was employed. The cutter was pressed against the surface of each specimen. The tester collar was rotated 3 complete revolutions (twelve 90 degree increments) and the readings recorded. The device was calibrated to read 100 with a 460 gram load indicating no penetration. Typically, this reading was done at 1, 3 and 24 hr after sample preparation.

Mold or green hardness indicates the resistance offered by the specimen surface to penetration by a loaded plunger. This result was reported in minutes as work and strip time. Timing was initiated upon addition of the final ingredient. The time elapsed until the gauge read 45 was taken as the work time. Timing continued until a reading of 90 was reached. The second time point was recorded as the strip time. A Simpson-Gerosa electronic mold hardness tester was used.

RESULTS AND DISCUSSION:

SOLVENT FOR LEVAN: Levan, like most bio-based polymers, is soluble in water but not in many other solvents. Although water solubility is often desirable from an environmental standpoint, moisture poses a problem for some applications such as in an iron foundry. Water removal is doable for processes using heat, but for a cold-box binder system, substantial amounts of water are unacceptable. A second goal was to find a solvent that evaporated more rapidly than water. Not all the solvents tested would have met this criterion but since no suitable solvent was identified, this was a moot point.

Levan is soluble in dimethyl sulfoxide (DMSO). DMSO is safe enough for use in veterinary pharmaceuticals but when subjected to the high temperatures of a foundry, sulfur compounds would be released. A recyclable version, piperylene sulfone, was considered, but it still contained sulfur which would be released upon heating.

Other than water, DMSO was the only solvent found for levan. Levan was found to not be soluble in the following:

- Methanol, ethanol, isopropanol, n-propanol, furfuryl alcohol
- Acetone, methylethylketone, toluene
- *d*-limonene
- Propylene carbonate, ethylene carbonate
- 1-vinyl-2-pyrrolidone
- Green solvents used for cleaning - EnSolve™, Asahiklin AK
- Methoxypolyethylene glycol, polyethylene glycol
- Kerosene, gasoline
- Dimethyl formamide
- Ethoxyethyl acetate, acetic anhydride
- Methyl soyate, ethyl lactate and other vegetable based solvents

When no suitable solvents were identified, the focus shifted to alternative approaches.

CHEMICAL CURING - MDI: No-bake and cold-box processes are common and are performed at ambient temperatures. To avoid expending energy to drive off excess water, chemical curing methods were examined.

Emulsifiable MDI: Phenolic urethanes are among the most widely used foundry binders in no-bake systems. A phenolic resin is reacted with diphylmethane diisocyante (MDI) to form the stable urethane. It was reasoned that substituting levan for the phenol would significantly reduce the toxicity of the formulation. A problem with using isocyanates in water borne systems is the reaction with the water rather than the hydroxyl groups on the resin. This problem has been addressed by a commercially available emulsifiable formulation. Hydrophilic surfactants with specific reactivity toward the MDI group are used to produce modified MDI variants. Interaction with water is minimized resulting in efficient cross-linking of the resin. The product used for experiments in this project is sold as Rubinate 1780 by Huntsman.

Cross-linking levan with MDI – initial tests: One part of levan was dissolved in two parts of water overnight. Rubinate is quite viscous while levan has an unusually low viscosity. Mixing them together in equal parts makes a solution that does not foam and blends easily with the sand. Sand coated with 3% (of the sand weight) levan and 3% (of the sand weight) MDI had about the right moisture content to permit easy packing in 50 gm molds. The molds were allowed to stand at room temperature. After 20 minutes, the forms had begun to set up. At 8 hours, the forms had hardened sufficiently to allow handling and they could not be manually broken after a 24 hour cure.

Catalyst – DABCO & DBTA: Although heating will certainly drive off the water and effect a more rapid cure, catalysts or alternative cross-linking agents may be needed to achieve the desired cure rate. One pair of catalysts tested was DABCO 33-LV, a triethylenediamine from Air Products, and DBTA (dibutyltin diacetate). To facilitate a more homogeneous coating, all of the liquids (levan, MDI and catalysts) were mixed together before adding the sand. This must be done very quickly since it would be undesirable to allow cross-linking to proceed for long before the sand is added. The catalysts react optimally at an alkaline pH while the Rubinate 1780 is acidic. The pH of the MDI was adjusted to 9.5-10 with sodium hydroxide. Although this should be optimal for the catalysts, it is not ideal for the MDI. It was found that mixing all of the liquids and the sand and then packing them into the mold needed to be accomplished within one minute. Longer times resulted in little or no bonding of the sand. As would be expected, the more catalyst, the faster the curing. Traditionally, DABCO and DBTA are used at a ratio of 10:1. It was found that equal amounts of the two catalysts worked better. The problem was that DBTA is quite expensive so this was not a practical formulation.

The initial set time is noted in the following table. By 8 hours, all samples could be carefully handled and by 24 hours none could be manually broken. This raised the question of whether the catalysts were needed. If forms could be dried or allowed to stand for 24 hours, there was not a huge difference in stability of the form with and without the catalysts.

DABCO (%)	0.0	0.4	0.4	4.0	4.0
DBTA (%)	0.0	0.04	0.4	0.4	4.0
SET TIME (MIN)	20.0	15.0	5.0	1.0	0.5

Figure 1: Ratios of catalysts tested with levan-MDI formulations. 4% DABCO and 0.4% DBTA gave a 1 minute set time but this high level of catalyst was too expensive to be practical.

Jeffamine D230, a polyetheramine with repeating oxypropylene units, DABCO EG and DABCO 33-LV, were tested but had no discernable effect.

Catalyst – Jeffcat DMDEE: Another type of catalyst, 2,2 dimorpholinodiethylether, was tested. This catalyst is available commercially as Jeffcat DMDEE from Huntsman.

Jeffcat DMDEE was used at rates ranging from 0.3 to 6.6%. Higher amounts of binder were used for the tests reported here simply because manual mixing seemed to require more binder. The lowest rates left the sand too dry in the manual mixing system, but other work indicates that the mechanical mixer allows the use of smaller amounts of liquids.

% LEVAN	% MDI	% DMDEE	WORK/STRIP TIME (MIN)	SCRATCH HARDNESS
2	5	5	1.5/6	6 min = 41 25 min = 45 50 min = 63
2	3	2	2.5/6.5	10 min = 71 1 hr = 75 3 hr = 77 24 hr = 82

Figure 2: In the manual mixing system, typical formulations shown resulted in reasonable work and strip times, but the scratch hardness did not reach suitable levels as quickly as required for a high through put system.

Flexibility: Glycerol was tested because some formulations were found to make brittle forms but glycerol added too much flexibility. It is possible that smaller amounts of glycerol could be useful. Other solvents (polyethylene glycol, polypropylene glycol, ethylene carbonate, and propylene carbonate) were also added in an attempt to provide sufficient moisture by fluids that would evaporate more quickly than water. No advantage was found in using any of these solvents.

pH: It was anticipated that pH adjustment would have a significant effect on some reactions. Several experiments run across the pH range had little or no effect. It is likely that the buffering capacity of the sand overrode pH adjustments of the binder.

Order of addition: It had been found that all liquids could be blended together for a more homogeneous mixture. The problem was that Jeffcat DMDEE increased the reaction rate so dramatically it was necessary to add the catalyst last after the sand had been coated with all the other reagents. The levan and MDI could be mixed prior to addition of the sand or the MDI could be used to dampen the sand where levan coated sand was used.

For the manual system, the one approach involved use of sand that had been coated with 2% levan and dried. Then emulsifiable MDI was mixed with the sand for 2 minutes to ensure complete dampening of the sand. Upon addition of 2% Jeffcat DMDEE, mixing was completed in 30 seconds and the coated sand packed into the form in the next 30 seconds.

Two methods were tried: (1) change the order of reagent addition and (2) protect the levan from an immediate reaction by coating it.

To examine the order of addition, an array was set up to cover all possible combinations (Table 3). Experiments based on this array were repeated twice for different rates of binder. The first row represents the standard approach of coating the sand with levan in water. Then adding the MDI and mixing again. Finally the catalyst (diluted in propylene carbonate for some experiments) was added prior to the final mixing.

LEVAN	MDI	DMDEE
1	2	3
1	3	2
2	1	3
2	3	1
3	2	1
3	1	2

Figure 3: Order of addition for levan, MDI and DMDEE catalyst.

The repeatable, significant effect seen was when the levan was added last (last two rows of table). Although the reaction was more rapid, the problem was the reaction was too fast and the material often hardened in the mixing container.

Slowing the reaction rate: Adding levan last increased the reaction rate, but to the point where it was not manageable. Three methods were tested for slowing down the reaction rate: (1) use sand that had been coated with levan and then dried prior to use, (2) coat the levan with clay and (3) divide the sand into two parts, coating each part and then combining the two portions of coated sand. The later two approaches were not successful. Using levan coated sand that had been dried, gave the best results returning to the standard order of addition and shown in the following table.

WORK TIME (MIN)	STRIP TIME (MIN)	SCRATCH HARDNESS			
		10 min	1 hr	3 hr	24 hr
2.5	6.5	71	75	77	82

Figure 4: Use of levan coated sand to slow reaction rate. Coated sand was mixed with 3% MDI. Then 2% DMDEE was added.

A method for coating sand with levan by spray drying was developed. To ascertain whether sand could be coated by mixing as effectively as by spray drying, sand was manual mixed with warm sand and a solution of levan with 1% glycerol added. Microscopic examination showed that the mixture was essentially homogeneous with an even coating on the sand particles. Photos of the manually mixed coated sand and the spray dry coated sand appeared similar. The manual method for coating the sand was used for all experiments reported here.

Coat the levan with clay: Others have used clay to decrease veining or porosity. 0.1% Laponite® (a synthetic, nanoclay from Southern Clay Products) was mixed with levan. The mixture was compared with levan alone that was cross-linked with several of the reagents

described above. Although no benefit was observed, it is believed this may still be a viable approach. Laponite® must be used at very low levels because of viscosity added to formulations. One possibility is to try other nanoclays. Another option would be to atomize the levan into a fine spray and coat those much finer droplets with the clay.

Two sand portions coated separately prior to combining them: For the third method, half of the sand was mixed with the MDI. Then the catalyst was added and mixing was repeated. In a separate container, the other half of the sand was mixed with the levan/water. Then both batches of coated sand were combined and mixing repeated. This approach was tried several times. Although the work time was increased, the bonding did not appear to continue and the forms never achieved good scratch resistance.

Mechanical mixing and additional testing: Using similar ratios of the binder components but at a total rate of only 1.5-2%, the formulations were tested at the Metal Casting Center using the mechanical mixing system. Levan was dissolved in water overnight. The following day ethanol was added. The final formulation was 33% levan, 45% water and 22% ethanol. The diluted levan was used at a rate of 25% with emulsifiable MDI used at a rate of 75%. The catalyst, Pep Set from Ashland, was used at 15%. Typical results are shown in the following table. At 1.5% total binder, tensile strengths as high as 162 psi were seen at 24 hrs. Work times were slightly shorter at 4 to 5 minutes; strip times were equivalent or slightly longer. Several formulations were made up with silanes but they were not found to be beneficial.

	TENSILE STRENGTH (PSI)			**SCRATCH TEST**
10 min	56		30 sec	79
1 hr	104		5 min	90
3 hr	144		1 hr	93
24 hr	133		3 hr	92

Figure 5: 25% levan-water-alcohol and 75% emulsifiable MDI binder was used at a rate of 2%. 15% Pep Set 3500 was the catalyst. The work time was 6 minutes and the strip time was 11 minutes.

CHEMICAL CURING - EPICHLOROHYDRIN: Although a levan-MDI formulation was less hazardous than phenol formaldehyde-based mixtures, it was recognized that also eliminating the isocyanate would be even more desirable. Attention turned to a cationic polyamidoamine-epichlorohydrin (PAE). PAE has been FDA approved and is used in paper towels, toilet paper and related products. Hercules produces a PAE under the name of Polycup. Numerous forms of Polycup are available and three were tested initially (172, 3160 and 6130). No distinct differences in activity were noted so one, Polycup 172, was selected and used for all the testing reported here.

Polycup 172 is heat activated. The manufacturer suggests using it at 245-350 F. The glass transition temperature for levan is around 265 F. Initial testing was done at 225 F but later experiments looked at the effect of higher temperatures. At 225 F using 3% levan in water, readings before 24 hours indicated limited hardening of the sand forms unless they were heated

for a full hour. The manufacturer indicates ring opening is initiated after only a few minutes at elevated temperatures so the need for prolonged heating here may reflect the need to remove water. Alternatively, the ring may be broken at a very high pH but this appeared impractical in the presence of the large amount of sand and earlier failures when pH changes had been examined.

OVEN TEMP (F)	TIME IN OVEN (MIN)	WORK TIME (MIN)	STRIP TIME (MIN)	SCRATCH HARDNESS				COMMENTS
				0 HR	1 HR	3 HR	24 HR	
250	5	1	>15		0	22	80	
250	15	0.5	1.5		87	86	83	
250	60	0	0		87	86	81	
325	5	0	10		0	71	79	
325	15	0	0		71	84	80	
325	60	0	1		76	58	55	Slightly caramelized
400	5	0	0		80	85	85	
400	15	0	0		83	81	80	Caramelized
400	60	ND	ND		ND	ND	ND	Charred
325	5	0	0	72	81	84	85	
325	15	0	0	84	77	84	74	
325	60	0	0		72	63	85	Slightly caramelized

Figure 6: This table shows the effect of activation temperature and time on cross-linking with PAE. Samples in the top section of the chart were prepared with 2% levan in water and 0.5% PAE. The binder was then mixed with uncoated sand. For samples in the bottom section of the chart (last three samples), sand was coated with 2% levan and dried before adding 1.24% PAE.

At 250 or 325 F, 5 minutes in the oven was insufficient when levan was added as a liquid. This may have as much to do with water removal as anything else since 5 minutes in the oven was sufficient using sand that had been pre-coated with levan and dried. 400 F was too high a temperature unless forms were left in the oven for 5 minutes or less. Even at 325 F, prolonged baking of 1 hour resulted in some breakdown of the levan as evidenced by the caramelization.

CHEMICAL CURING - MELAMINE AND TITANATE:

Other catalysts were tested including a modified melamine (Cymel from Cytec Industries) and an organic titanate (Tyzor LA from DuPont). All liquids were mixed together before the sand was added. Although no samples could be broken manually after a 48 hour room temperature cure, no advantage was seen. It is possible that heating could improve the results.

Leven without additivesS:

The most environmentally friendly option is to use levan alone, with no catalysts, cross-linkers or any other additives. This approach will tend to be the least toxic for foundry employees, among the more environmentally friendly methods and may minimize costs. While this approach is possible, the experiments done to date indicate that some heat may be required for any process where cores must be strong enough for handling in a very short period of time. The shell process may be one application where levan could be used without additives.

Levan is produced by fermentation. The first sample of levan sent to the University of Northern Iowa Metal Casting Center was not as highly purified as the later product. It also contained some ethanol. A complete analysis of the early material was not available, but based on testing of later batches and the increased number of purification steps, it is estimated that the original product had around 1-3% fat, 1-2% protein and 2-4% ash. The amount of ethanol has been estimated at around 25-35%. Solutions of more than 50% ethanol are known to precipitate levan. The initial testing indicated this unpurified levan in a water-ethanol solution could be used as a binder with no other additives.

Tests reported here used a more purified levan, with and without ethanol added. Initially, rates of levan and alcohol were varied and the forms dried in an oven at 250 F. 3% levan/water + 4% ethanol (w/w) dried for one hour produced forms that had reached full strip time upon removal from the oven. It reached and maintained full scratch hardness at 1 to 24 hrs. Decreasing the amount of levan to 1.5% and the ethanol to 2% gave similar results after only 10 min in a 250 F oven. 1.5% levan and no ethanol accompanied by drying for 10 or 60 minutes at 250 F, gave full strip time upon removal from the oven but scratch hardness ranged from 41 to 58 for the 1, 3 and 24 hour readings with no apparent pattern.

% LEVAN	TEMP F	SCRATCH HARDNESS		
		1 HR	3 HR	24 HR
2	76	0	0	51
2	225	80	87	84
3	76	0	0	76
3	225	85	84	83
4	76	0	0	67
4	225	82	86	80

Figure 7: 225 F for 1 hr resulted in cores of moderate hardness for samples bonded with levan in a water-alcohol solution but with no other additives.

Initial testing at the University of Northern Iowa had not involved drying the forms in the oven. Having some indication that the alcohol did have a role, the next series of experiments were done with no drying. One of the earliest methods used for purification and recovery of polysaccharides involves precipitation with alcohol. Many of these procedures call for addition of "ice cold" alcohol and some also cool the aqueous solution of the desired polysaccharide. Here we theorized that replacing as much water as possible with alcohol might increase the reaction rate. For all earlier testing, ethanol had been added at ambient temperature. Here both the diluted levan and the ethanol were heated to either 45 or 50 C. As can be seen in the following table, a change of only 5 F had a significant impact on the results. Holding the temperature the same and doubling the rate of use of levan resulted in the difference between a zero scratch hardness and a 73 at 24 hours.

LEVAN/ WATER	LEVAN % IN LIQUID	ETOH % W/W	TEMP (F) WHEN ETOH ADDED	% LEVAN IN SAND	WORK TIME (MIN)	STRIP TIME (MIN)	SCRATCH HARDNESS	
							1 HR	24 HR
1/1	32	35	113	0.6	45			0
1/1	32	35	113	1.2	47			0
1/1	34	31	122	0.6	40	140	0	0
1/1	34	31	122	1.4	39	149	13	73

Figure 8: Use of levan/water/ethanol as binder with no other additions. The binder was held at 113 or 122 F.

Temperature will affect the amount of alcohol that can be blended with a levan/water solution before the levan precipitates and additional trials are needed to establish the optimum temperature and ratio.

There are a lot of other factors that influence precipitation by the alcohol process. Use of various alcohols will make a significant difference. For levan, precipitation with methanol or acetone gives a hard lump of levan while precipitation with ethanol is more apt to give a product that is much more pliable.

LEVAN/ WATER	LEVAN %	ETOH %	TEMP F	TIME IN OVEN MIN	WORK TIME	STRIP TIME	SCRATCH HARDNESS		
							1 HR	3 HR	24 HR
1/2	3	4	250	60	0	0	85	85	82
1/2	1.5	2	250	10	0	0	87	87	85

Figure 9: Heating sand cores bonded by levan in water/ethanol at 250 F for only 10 min, resulted in samples that had already reached strip time upon removal from the oven and maximum scratch hardness at only 1 hr.

A similar formulation was tested at the Metal Casting Center. A solution of 27% levan, 36.5% water and 36.5% ethanol produced a sample with a 10 min tensile strength of 60 psi and 24 hr tensile strength of 170 psi. Samples had an average strip time of 11 min, a moderate performance.

To a certain extent, the same effects can be duplicated by varying the alcohol concentration. Although not yet studied, it is possible that a more pliable precipitate may do a better job of binding than the stiffer product seen at higher alcohol concentrations or from methanol. pH and salt concentrations may also have an effect. The first sample that was tested at the Metal Casting Center contained more impurities than the production material. The purification techniques have been improved. The current batch does have 0.86% fat, 0.51% protein and 2.1% ash. Although these numbers are small, they may have been somewhat higher in the first batch. Protein is certainly one factor to be considered as having had a role in the binding process.

Accomplishments:

Formulations for foundry binders that were far less toxic than widely used phenol formaldehyde binders were developed and tested. Replacing part or all of traditional binders with levan made specimens with reasonable but not commercially viable properties. Chemically curing methods offered energy savings over heating. For processes using heat anyway, the use of epichlorohydrin to cross-link levan actually hardened too rapidly. Backing off on the cure time or temperature may offer a workable method. The addition of ethanol to an aqueous solution of levan generally produced specimens with improved hardness and tensile strength.

The most environmentally friendly method used levan alone. Although this approach may not be suitable for a no-bake process, it has been suggested that levan might be used in a shell process. Two methods for producing levan-coated sand were tested and were viable on a laboratory scale.

Reccomendations:

1. Optimization of conditions for cross-linking levan with polyamidoamine-epichlorohydrin (PAE).

2. Investigate variables affecting hardness and tensile strength of cores bonded with levan alone. Levan should be prepared with a simple one-step recovery and no purification. This will leave the protein, fat and ash in the raw levan which may be critical to its sand binding capacity. Use of a non-purified fermentation product will have the added advantage of decreasing the cost. Other variables to be examined include pH, temperature and the type and concentration of alcohol.

3. Test levan as a binder in a shell mold process.

Section 3- Mathematical modeling of gas emissions from urethane bonded sand molds.

1. Project Executive Summary

An emission model was proposed and incorporated into a casting simulation model to predict the production rate and transport of pyrolysis components of a biodiesel phenolic urethane binder in a mold. Casting experiments did not confirm the validity of the mold/core gas model but shed light on the complex reactions occurring inside the mold influencing the resultant emission into the workplace environment. The TGA pyrolysis approach and GC-MS originally used for data collection of pyrolysis species and production rate conclusively showed the initial reaction mechanisms of the decomposition of phenolic urethane. Because of the substantial release of benzene observed in the validation experiments, the initial pyrolysis species of the decomposition of phenolic urethane is suspected to contribute significantly to benzene generation during casting.

The research work accomplished the majority of proposed tasks and milestones. During the course of the research program, several challenges were encountered. In the analytical data collection approach using TGA and GS-MS techniques, the Casting Emission Reduction Program (CERP) as a source for identifying a dozen major HAP and VOC chemical species constituting a substantial amount of emissions during the casting process. The researchers observed during the course of the model development that a significant portion of the emission was unaccounted for in the mass balance, leading to a constant mass assumption during simulation. The casting validation experiment strongly indicates these “other” pyrolysis species contribute significantly to the overall emission rate into the workplace environment.

It also apparent from the validation casting experiments that the condensation and vaporization model needs to be modified to consider potential secondary gaseous reactions. The model considers the production of HAP’s and VOC’s to be solely from the decomposition of the phenolic urethane binder. The species was assumed to move away from the heat, condense in cooler regions of the mold, and vaporize if the temperature field rises above the vaporization point. This modeling approach is valid for water condensation in green sand molds. However, if the gas velocity is sufficient low compared to the moving temperature field or the pyrolysis species remain stationary for a sufficient period of time, secondary decomposition reactions can occur leading to further decomposition of larger benzene derivative molecules.

The researchers recommend the following suggestions for further research in the complex degradation of chemical binders used in the casting process. At the present time, the mold gas velocity component for the transport of the pyrolysis species is not a well-known variable and

future research work should explore this critical parameter to develop a robust condensation and vaporization model. The condensation/vaporization model needs to consider potential decomposition reaction of complex benzene type molecules under a reducing atmosphere. An expanded and detailed experimental research is recommended using the TGA and GC-MS approach for a complete pyrolysis species accountability under a variety of heating rates. In addition, to support the condensation and vaporization model, possible gaseous secondary reaction leading to benzene production should be considered during further model development and future development of an experimental plan.

Simulation of pyrolysis components during thermal degradation and decomposition of chemical binders during casting has a significant role for the U.S foundry industry. Emission into the foundry workplace environment and subsequent release into the surrounding community plays a significant economic and sustainability factor for the viability of the American foundry. Prediction of emission can offset large emission sources that exceed government regulation by allowing casting designers to foster better thermal management of the casting process. In addition, the emission model can also support casting quality issues such as gas defects and metal penetration by predicting areas of concentrated gas generation and identifying possible solutions to meet these potential quality challenges. Working with the foundry industry and software vendors, the emission model is planned to be developed further to foster a robust simulation tool that can be used by casting designers.

2. Introduction

During the casting process, large temperature gradient inside the mold produces variable conditions for the decomposition of polymer based resin systems, determining the type of emitted compounds based on whether it is directly related to the decomposition or decomposition of high molecular weight condensable products. Immediately at the casting interface, the extremely hot metal comes in contact with the mold surface, inducing an extremely high thermal gradient. As the heat is transferred from the casting interface, the thermal gradient significantly changes because of the thermal resistance of the mold material. The transient thermal profile developed in the mold will reach stabilization, producing variable heating rates as a function of distance from the mold-metal interface. The rise in temperature will lead to chemical changes in the polymer binder followed by the subsequent decomposition into lower molecular weight compounds, usually carbon residue, greenhouse gases, and complex gases.

The decomposition of the resin binders is a multifaceted reaction. Researchers such as McKinley et al[2] and the extensive subsequent work by the Casting Emission Reduction Program have measured the complex gas species emitted from the casting process for almost every type polymer binder system and green sand molding methods. The information collected provides a baseline for emitted hazardous air pollutants (HAP's) and volatile organic compounds (VOC's), though the information is more a snapshot of the total emitted amount over a standard measurement time frame and casting configuration. It is widely accepted by industry that casting configuration and mold wall thickness will dramatically affect these baseline values, skewing the total amount of emitted compounds dependent on the casting facility poured metal and molding practice. Because of the almost infinite casting parameters induced by the casting process, emission products from casting facilities is highly variable resulting in changes by metalcasters in the casting process to meet emission standards. Emission strategies results in downstream difficulties that consume additional energy usage for additional post processing to correct casting defect problems induced to meet environmental regulations.

Simulation tools are practically used in all metal casting operations today. Designs can be verified to meet casting performance and metallurgical quality. Unfortunately, these tools are not very effective in assessing potential defects cause by the mold, especially when new foundry products such as resin binders are introduced into the casting process. General discussion with the foundry industry indicated an estimated 60% of scrapped castings are a result of the mold, with the primary source of casting defects being gas related. Research has been conducted to understand the physical aspect of gas generated defects but the rudimentary

approach does not identify the true source of these emitted compounds or how the continued heating of the sand effects gas production. Additionally, the physically treatment of this phenomenon does not provide any solutions to the environmental concerns of the decomposition of polymer based binder systems.

Development of a simulation tool to include the source generation of emitted compounds has a tremendous benefit to the foundry industry by providing upfront energy saving strategies to reduce casting defects while understanding the environmental impact of the casting process. Based on fundamental principles of physical characteristics and empirically measured thermal parameters, understanding the decomposition of binder systems can lead to integration of casting simulation tools into a total energy management strategy approach of the casting process from the design to final casting. Modeling of binder decomposition and gas generation identifies potential gas generation sources that contribute to energy intensive secondary processing techniques such as welding and grinding or, in the case of excessive damage, subsequent remelting of casting from scrapping.

3. Mold/Core Gas Model

The binder degradation model developed in this project simulates the pyrolysis of mold/core sand binders during metal casting. This model is incorporated within a larger multi-component, porous medium simulation model of gas in core and mold sand regions that is currently being developed in the commercial casting simulation software package MAGMASOFT [1]. The current implementation of MAGMASOFT predicts (among other things) the temperature distribution throughout the casting process, both in the metal as well as in the surrounding mold/core regions. The temperature predictions in the mold and core regions are utilized in the porous medium simulation model being developed by MAGMASOFT to predict gas evolution and flow in the mold/core regions during casting. The gas phase may consist of ambient gases, greenhouse gases, hazardous air pollutants (HAPs), water vapor, and other components. The fundamental equations of the MAGMASOFT mold/core gas model consist of a mass conservation equation for each component, Darcy's Law for the gas phase flow, an overall volume balance equation that determines the pressure distribution, and an energy balance equation that determines the temperature distribution throughout the mold and core sand. These equations account for the compressibility of gases as well as for condensation and/or vaporization. This section briefly describes the equations in the MAGMASOFT mold/core gas model, ending with a description of the binder degradation (pyrolysis) model developed in this project.

3.1 Gaseous Species Conservation

In the gas phase, the mass of each gaseous component i is determined by enforcing the following species conservation equation:

$$\frac{\partial C_i}{\partial t} + \nabla \cdot \left(\rho_i \hat{C}_i \boldsymbol{u} \right) - \nabla \cdot \left(\phi \rho_i D_i \nabla \hat{C}_i \right) = R_i, \qquad i = 1,..., N \tag{1}$$

where N is the number of gaseous components; C_i is the mass of component i per unit total volume (i.e., sand plus gas phase volume); $\hat{C}_i$ is the volumetric concentration of component i per unit gas phase volume (note that $\sum_{i=1}^{N} \hat{C}_i = 1$); t is time; ϕ is the sand porosity; ρ_i is the density of gaseous component i (determined using the ideal gas law); D_i is the molecular diffusion of component i; R_i is the production rate of component i, which may occur due to pyrolysis or condensation/vaporization; and $\boldsymbol{u} = \phi \boldsymbol{U}$ is termed the superficial gas phase velocity, where $\boldsymbol{U}$ is the velocity.

3.2 Gas Velocity

The velocity of the gas phase is determined using Darcy's law, which states that flow through a porous media (i.e., sand) is governed by the following equation:

$$\boldsymbol{u} = -\frac{K}{\mu_g} \left(\nabla P - \rho_g \boldsymbol{g} \right) \tag{2}$$

where K is the sand permeability; μ_g is the dynamic viscosity of the gas phase, given by $\mu_g = \sum_{i=1}^{N} \hat{C}_i \mu_i$; ρ_g is the density of the gas phase, given by $\rho_g = \sum_{i=1}^{N} \hat{C}_i \rho_i$; $\boldsymbol{g}$ is the gravity vector; and P is the pressure of the gas phase.

3.3 Gas Pressure Equation

If species conservation equations (e.g., Equation (1)) are summed over all species, an overall mass conservation equation results. This mass conservation equation can be combined with Darcy's law, given in Equation (2), to produce the following pressure equation for the gas phase:

$$-\sum_{i=1}^{N} \frac{1}{\rho_i} \nabla \cdot \left(\rho_i \hat{C}_i \boldsymbol{u} \right) + \kappa_g \frac{\partial P}{\partial t} + \beta_g \frac{\partial T}{\partial t} = \sum_{i=1}^{N} \frac{R_i}{\rho_i} \tag{3}$$

where β_g is the gas phase expansion coefficient, given by $\beta_g = \sum_{i=1}^{N} C_i \beta_i / \rho_i$;and κ_g is the gas phase compressibility, given by $\kappa_g = \kappa_s \phi + \sum_{i=1}^{N} C_i \kappa_i / \rho_i$, where κ_s is the sand compressibility.

3.4 Energy Equation

Assuming that the sand and the gas phase are in thermal equilibrium, conservation of energy can be written as:

$$\frac{\partial}{\partial t}\left\{\left[(1-\phi)\rho_s c_s + \sum_{i=1}^{N} c_{p,i} C_i\right] T\right\} + \nabla \cdot \boldsymbol{J} = T \sum_{i=1}^{N} c_{p,i} R_i \tag{4}$$

where ρ_s and c_s are the density and specific heat of the sand, respectively, and $c_{p,i}$ is the specific heat of gaseous component i. The heat flux, $\boldsymbol{J}$, is given by:

$$\boldsymbol{J} = \boldsymbol{u} T \sum_i \rho_i c_{p,i} \hat{C}_i - \left[(1-\phi) k_s + \phi \sum_{i=1}^{N} \hat{C}_i k_i\right] \nabla T \tag{5}$$

where k_s is the thermal conductivity of the sand, and k_i is the thermal conductivity of component i. The first term on the right-hand side of Equation (5) accounts for convection, and the second term accounts for conduction. Equation (4) can be solved to determine the temperature distribution throughout the mold/core regions during casting.

3.5 Condensation/Vaporization Model

As heat from the melt penetrates into the mold/core sand, evaporation of water or condensed reaction products may occur. These and other gaseous products may then be transported to cooler regions of the mold/core, where they may condense. Condensation and vaporization are important to consider when modeling mold/core gases. In particular, gas emissions are overestimated if condensation of binder degradation products is not considered.

The net mass production rate of condensation/vaporization of gaseous component i is given by the following equation:

$$R_i = S_p k_m \rho_i \left(\frac{P_i^{sat}}{P} - \hat{C}_i\right) \tag{6}$$

where S_p is the specific area of the sand; k_m is the mass transfer coefficient; and P_i^{sat} is the saturation pressure for component i. If $P_i^{sat} > P\hat{C}_i$, then R_i is positive (recall that R_i is the

production rate term in Equations (1), (3) and (4)), and evaporation occurs. If $P_i^{sat} < P\hat{C}_i$, then R_i is negative, and condensation occurs.

3.6 Pyrolysis Model

The binder degradation model developed in this project is based on the work of McKinley et al.[2] The model is derived from the following pyrolysis rate equation:

$$\frac{\mathrm{d}f}{1-f} = \frac{k}{\beta}\mathrm{d}T \tag{7}$$

where T is the absolute temperature; $\beta = dT/dt$ is the heating rate; f is a normalized mass, $f = (m_0 - m)/(m_0 - m_f)$, where m, m_0 and m_f are the current, original and final sample masses, respectively; and k is a reaction rate coefficient. For a single pyrolysis reaction, k can be modeled as a function of temperature by the following Arrhenius equation:

$$k = A\exp\left(-\frac{E}{\overline{\mathrm{R}}T}\right) \tag{8}$$

where $\overline{R}$ is the universal gas constant ($\overline{R} =$ 8.314 kJ/kmol-K); A is the frequency factor for the reaction; and E is the activation energy for the reaction. Substituting Equation (8) into Equation (7) and integrating the result, the following expression is obtained:

$$\frac{\mathrm{d}(m/m_b)}{\mathrm{d}T} = -\frac{A}{\beta}\left(\frac{m_0 - m_f}{m_b}\right)\exp\left[-\frac{A\overline{\mathrm{R}}T^2}{\beta E}\left(1-\frac{2\overline{\mathrm{R}}T}{E}\right)\exp\left(\frac{-E}{\overline{\mathrm{R}}T}\right) - \frac{E}{\overline{\mathrm{R}}T}\right] \tag{9}$$

where m_b is the original binder mass. Note that m_b is different from m_0. The original and final values m_0 and m_f are with respect to a single pyrolysis reaction. Binder degradation is the result of many different pyrolysis reactions. Thus the original sample mass, m_0, is only equal to the original binder mass, m_b, for the first pyrolysis reaction that occurs. The original mass for subsequent pyrolysis reactions is some value smaller than m_b.

For each peak in a given pyrolysis production rate curve, values of A, E and $(m_0 - m_f)/m_b$ in Equation (9) can be optimized to produce a model curve that best fits this peak in the production rate curve data. By performing this operation for each peak in a pyrolysis production rate curve and summing the resulting model curves, the entire production rate curve can be modeled, yielding the following equation representing the total degradation of the binder mass:

$$\frac{\mathrm{d}(m/m_b)}{\mathrm{d}T} = \sum_{j=1}^{M} -\frac{A_j}{\beta}\left(\frac{m_0 - m_f}{m_b}\right)_j \exp\left[-\frac{A_j \overline{\mathrm{R}} T^2}{\beta E_j}\left(1 - \frac{2\overline{\mathrm{R}}T}{E_j}\right)\exp\left(\frac{-E_j}{\overline{\mathrm{R}}T}\right) - \frac{E_j}{\overline{\mathrm{R}}T}\right] \quad (10)$$

where M is the total number of peaks in the pyrolysis production rate curve.

The peaks in a pyrolysis production rate curve are seen in the next section to correspond to the evolution of individual pyrolysis products. Therefore, in addition to the overall pyrolysis production rate curve modeled in Equation (10), the production rates of each pyrolysis product are known as well from Equation (9). This information is used to determine for each pyrolysis product the production rates, R_i, used in Equations (1), (3) and (4), thus enabling the MAGMASOFT mold/core gas model to incorporate binder degradation products.

4. Measured Pyrolysis Data

The measured pyrolysis data utilized to develop the current pyrolysis model parameters was gathered in experiments performed at The Pennsylvania State University[3]. Sand core samples containing 1.5 wt% biodiesel phenolic urethane binder were utilized for all measurements. Both flash pyrolysis and thermogravimetric analytical (TGA) slow pyrolysis were conducted on core samples. The present model utilizes only the TGA results, which are more representative of heating rates in the bulk of sand cores (i.e., except very near the core/metal interface).

4.1 TGA pyrolysis emission analysis for total amounts of pyrolysis products

15 grams of core sample (1.5% core binder) was pyrolyzed in a TGA (Cahn TG-131, Thermo Electron Inc., CA) with a heating rate of 10 ^{o}C/min from ambient temperature to 900 ^{o}C under N_2. During the heating, granular activated carbon (GAC) tubes or Tedlar air sampling bags (Supelco, Bellefonte, PA) were used to collect the TGA emissions in the TGA effluent.

The GAC captured emissions were analyzed following the EPA method 18 that measures gaseous organic compound emissions. The GAC captured emissions was extracted with carbon disulfide solvent for 24 hrs. Then the solvent with analytes was analyzed for volatile hydrocarbons (hydrocarbons that host 6 to 16 carbon atoms) by a gas chromatography-flame ionization detector (GC-FID) (Hewlett-Packard 5890 Series II, packed column inlet with a 100% dimethyl polysiloxane colume). The identification and quantification of compound peaks were conducted by comparing the sample retention times and peak areas with those of standard solutions.

Methane, CO and CO_2 emissions were analyzed for the TGA emission samples collected by the Tedlar air sampling bag. 1 mL of the gas sample was injected into a GC (Shimadzu GC-17A). The GC was equipped with a FID for hydrocarbon analysis and a thermal conductivity detector (TCD) for CO and CO_2 analysis. The identification and quantitation of compound

peaks were conducted by comparing the sample retention times and peak areas with gas standards (Supelco, Bellefonte, PA).

4.2 TGA pyrolysis -mass spectrometer (MS) analysis for continuous pyrolysis analysis

About 400 mg of core sample (1.5% core binder) was placed in a TGA 2050 (TA Instruments, Newcastle, DE) and pyrolyzed from ambient temperature to 1000 ^{o}C with a heating rate of 10 ^{o}C/min under an argon atmosphere. This simulated some key features of the slow heating conditions that the core experienced at distances that were further away from the metal-core interface. The gaseous effluent from the TGA flowed to a downstream mass spectrometer (Thermostar GSD 301T, Pfeiffer Vacuum Inc., Nashua, NH) for emission kinetics analysis. For species identification, the mass spectra were compared to those in the NIST Mass Spectral Library (Chem SW, Version 2.0, Fairfield, CA, USA). ^{38}Ar isotope of the carrier argon gas served as an inner standard. The MS intensities were normalized to the intensities of ^{38}Ar isotope to eliminate errors caused by a shift in the MS sensitivity, and then normalized by the mass of the core samples.

4.3 Pyrolysis Results and Correlation

Figure 1 shows the total binder mass and pyrolysis rate as functions of temperature for the second pyrolysis sample, where both quantities are given relative to the original binder mass (OBM). The binder mass begins to decrease at about 80°C. Once the sample reaches 1000°C, only about 20% of the original binder mass remains. The pyrolysis rate is highest below 500°C, dropping to a nearly constant, lower value above 500°C. Table 1 lists the amount of pyrolysis products collected and measured over the entire heating range for the first sample. These values represent total captured emissions for each gaseous species measured. Note that the total amount of products collected in Table 1 is 142.2 mg/g binder. The total amount of binder mass consumed in the pyrolysis of the first sample was 766.7 mg/g, indicating that the data in Table 1 only accounts for about 20% of the total binder mass consumed. The remainder of the mass was reported to be water vapor (which was not measured) and gaseous pyrolysis products that re-condensed in the TGA apparatus.

Figure 2 shows the amount of greenhouse gases collected, as a function of the temperature intervals over which they were emitted, during the pyrolysis of the first sample. Carbon dioxide is released primarily below 450°C, and methane and carbon monoxide are released primarily above 450°C. Figure 3 shows mass spectrometry results for individual pyrolysis product species as a function of temperature. For each species shown in the figure, this kinetic data indicates the relative amounts of that species generated via pyrolysis, as a function of temperature.

Note that the kinetic data in Figure 3 are given in terms of normalized current. This kinetic data can be converted to a weight fraction (%OBM) by combining the data in Figure 3 with the data in Table 1. For example, consider the benzene data shown in Figure 3. This curve is repeated in Figure 4a. The area under this curve, integrated up to any given temperature (after shifting the curve so that the smallest value is zero on the normalized current scale), indicates the fraction of the total amount of benzene released up to that point. At 1000°C, all of the benzene represented by the normalized current curve has been released, and thus the integrated response reaches 100%. This integrated curve is also shown in Figure 4a. From Table 1, the total amount of benzene captured during TGA pyrolysis of the first sample was measured to be 1.258 mg/g binder. If the value of 100% on the right vertical scale of Figure 4a is equated to 1.258 mg/g binder, then Figure 4a can be re-scaled in terms of %OBM. This is shown in Figure 4b. The absolute value of the derivative of this curve gives the benzene production rate, in %OBM/°C; this curve is also shown in Figure 4b. These operations were performed for the six HAP gas species and the two 'Other Emissions' species listed in Table 1, providing production rate data in terms of mass fraction for these eight species. The greenhouse gas data in Figure 2, already given as mass fractions, was converted to cumulative mass generation with increasing temperature data (similar to Figure 4b), and the derivative of these curves was taken to produce production rate curves for each of the three greenhouse gases listed in Table 1. Thus, production rate data as a function of temperature was then available in terms of mass fraction for all eleven species shown in Table 1. This production rate data, along with the total pyrolysis data shown in Figure 1, is used in the next section to derive the parameters for the present pyrolysis model.

5. Development of Pyrolysis Model Parameters

As mentioned in Section 1.6, optimum values of A, E and $\left(m_0 - m_f\right)/m_b$ in Equation (9) were determined to produce model curves that best fit the peaks in production rate curves, such as the benzene production rate curve shown in Figure 4b. To illustrate this process, the benzene production rate curve is repeated in Figure 5a. This curve was modeled using two different peaks. The parameter values for these peaks are:

Peak 1: $A_1 = 300\ \text{min}^{-1}$; $E_1 = 8{,}500$ cal/mol; $\left[\left(m_0 - m_f\right)/m_b\right]_1 = 0.01132$

Peak 2: $A_2 = 20{,}000\ \text{min}^{-1}$; $E_1 = 19{,}250$ cal/mol; $\left[\left(m_0 - m_f\right)/m_b\right]_1 = 0.11447$

These two model peaks are shown along with the benzene production rate curve in Figure 5a. These peaks can be superimposed by summing the peaks using Equation (10). The sum of these two peaks is shown along with the benzene curve in Figure 5b. This figure shows that the model for the benzene production rate curve is in good agreement with the measured curve.

This same procedure was performed for all 11 species listed in Table 1, producing model production rate curves for each species, analogous to the model curve in Figure 5b for benzene. Thus, the binder degradation model provides production rates for greenhouse gases and HAPs, in particular, as functions of temperature. This information is utilized in the MAGMASOFT model to determine the production source terms in Equations (1), (3) and (4).

In addition to modeling the production rates for each of the 11 species in Table 1, the total binder mass and pyrolysis rates are also of interest. Modeling these quantities begins by summing the model production rate curves of the 11 species from Table 1, using Equation (10). This produces a pyrolysis rate that accounts for all 11 of these species. Furthermore, by integrating this 11 species pyrolysis rate curve over the temperature range, it is possible to determine the amount of pyrolysis products produced by these 11 species (which is equal to the original binder mass minus the binder mass lost due to these 11 species). The modeled curves for the pyrolysis rate and binder mass for the 11 species in Table 1 are shown in Figure 6, along with the total binder mass and total pyrolysis rate curves. As discussed in Section 2, the binder mass lost due to the 11 species in Table 1 only accounts for about 20% of the total binder mass loss, with the remaining 80% being due to water vapor production and condensation of pyrolysis products, neither of which were accounted for in the experiments. This is reflected in Figure 6, where the pyrolysis rate due to the Table 1 species is smaller than the total pyrolysis rate, and the binder mass lost at 1000°C due to the species in Table 1 is far less than the total binder mass lost.

The binder mass data in Figure 6 is re-plotted in Figure 7 as pyrolysis products generated (again in %OBM). The percent of pyrolysis products generated is simply 100% minus the binder mass lost (i.e., at any temperature, the sum of the remaining binder mass and the pyrolysis products generated to that point must equal the original binder mass). Again, this figure shows that the pyrolysis products generated due to the 11 species in Table 1 only account for only about 20% of the total amount of pyrolysis products generated by 1000°C. The third curve given in Figure 7, labeled ‘other’ pyrolysis products, is simply the total pyrolysis products curve minus the pyrolysis products due to the Table 1 species curve. In other words, this curve accounts for all pyrolysis products not generated due to the Table 1 species. Taking the derivative with respect to temperature of this ‘other’ pyrolysis product curve gives the production rate of ‘other’ pyrolysis products. This ‘other’ production rate curve is plotted in Figure 8, along with the ‘other’ pyrolysis product curve, re-plotted representing this data as binder mass lost rather than as pyrolysis products generated (i.e., ‘other’ binder mass lost = 100% - ‘other’ pyrolysis products generated). As with the production rate curves for the individual species listed in Table 1, this ‘other’ production rate curve in Figure 8 can be modeled as a series of peaks using the present pyrolysis model. This is shown in Figure 9,

where the ‘other’ production rate curve is shown along with the modeled production rate curve that was generated by summing 8 different peaks.

Adding the production rate curves for the 11 species in Table 1 to the production rate curve for the ‘other’ species shown in Figure 9 (using Equation (10)), the total production rate is determined. This modeled total production rate (pyrolysis rate) curve is compared to the measured pyrolysis rate curve in Figure 10a, where the curves are seen to be in reasonable agreement. If the area under these curves is integrated, the result is the total amount of pyrolysis products generated as a function of temperature. Subtracting the total pyrolysis products generated from the original binder mass provides the amount of binder mass remaining. The modeled curve representing the remaining binder mass is compared to the measured values in Figure 10b. Good agreement between the modeled and measured binder mass as a function of temperature is seen.

Using the model described here, the production rates of the 11 species in Table 1 (as well as the production rate of all ‘other’ species not taken into account in Table 1) can be predicted as functions of temperature. In addition, the total pyrolysis rate and the remaining binder mass can also be predicted as functions of temperature. Incorporating this binder degradation model into the mold/core gas model described in Section 1, it is possible to simulate binder degradation, as well as the motion and condensation of pyrolysis products within the mold and core regions, within casting simulation software. Two examples of such simulations are given in the next section.

6. Mold/Core Gas Simulation Examples

The model described herein has been used to simulate mold/core gases in two examples. The first example is a one-dimensional (1-D) sand sample, while the second example is a small tree core. Both examples model sand with 1.5 wt% biodiesel phenolic urethane binder (i.e., phenolic urethane cold box (PUCB)).

6.1 One-Dimensional Sand Sample Simulation

The first simulation involves a 10 x 10 x 20 cm sand sample (initially at 20°C) heated from one side at a constant temperature of 1000°C (see Figure 11). The opposite side is an outlet through which gases could escape. The other four faces use symmetry boundary conditions, such that the problem is essentially 1-D. The original binder mass concentration is 14 kg/m^3 of sand. The simulation time is 1000 s. Figure 12 shows temperature profiles at various times throughout the simulation. The temperature is seen to rise near the heated end of the sand. Note that even by 1000 s (Figure 12d), only about 25% of the sand is heated above 200°C, and more than half of the sand is below 50°C. Figure 13 shows binder mass concentration profiles

at the same times that were shown in Figure 12. The binder mass concentration drops to about 7 kg/m^3 near the heated end. Except near the heated face, the binder mass in most of the sample remains near the initial value of 14 kg/m^3 because the temperature is not high enough to initiate significant pyrolysis of the binder. Figure 14 shows corresponding distributions of the gaseous cresol created as a result of pyrolysis (shown in units of volume fraction of the gas phase). Note from the scale that the amounts of cresol are small. Cresol is generated near the heated face, and then moves toward the outlet as it is carried via gas phase motion. Finally, Figure 15 shows the liquid cresol that is created due to condensation of gaseous cresol moving from hotter sand to regions of cooler sand away from the heated face.

Figure 16 shows plots of the total binder mass and the overall pyrolysis rate in the sand sample as functions of time. Note that only a small portion of the original binder mass is consumed by 1000 s (mass drops from 0.037 kg to 0.033 kg). The absolute value of the time derivative of the binder mass curve gives the overall pyrolysis rate given in Figure 16. This rate curve shows peaks and troughs as various pyrolysis species are created.

Figure 17 shows the mass of gases that are emitted from the outlet face of the sand sample during the simulation. Figure 17a uses a mass scale that shows the three most prevalent gases: air, 'other' and CO_2. Air is the gas that existed in the mold at simulation time zero. This gets driven out of the mold as pyrolysis products are created. Note that after about 700 s, the amount of air stops changing; this is because it has all exited the sand sample at this point. The next most prevalent gas is the 'other' species, followed by CO_2. The amounts of both of these species are still increasing at the end of the simulation. Figure 17b shows the same data, using a smaller mass scale to illustrate the other gas species emissions. Figure 17 illustrates that the mold/core gas model is capable of determining the amount of emissions that escape from the mold/core during casting.

6.2 Tree Core Simulation

The second example is the heating of the 1 cm-thick tree core shown schematically in Figure 18. The core, initially at 20°C, is surrounded by liquid metal that is assumed to be at a constant 1000°C. Core heating and mold/core gas modeling are simulated for 80 s. The original binder mass concentration is 14 kg/m^3. Figure 19 shows temperature contours for the core at different times during the simulation. The bulk of the core exceeds 500°C by 80 s, and thus the majority of pyrolysis is complete by the end of the simulation (see Figure 1). Figure 20 shows pressure contours in the tree core at various times during solidification. Note that as the core temperature rises and pyrolysis products are produced, the pressure in the core also rises, except at the outlet where the pressure remains at atmospheric. The highest pressures are seen at 20 s. After this time, the pressure begins to decrease in the core as pyrolysis slows. Binder

mass concentration contours are shown in Figure 21. These contours show the progress of binder degradation as time progresses, ending with binder mass concentrations at about half of their initial value. Finally, Figure 22 shows contours of the CO_2 pore volume fraction at various times. Note that very little CO_2 is present at 20 s; however, that the amount begins to increase by 40 s. This simple example demonstrates the capabilities of the mold/core gas model to simulate core/mold gases during casting.

7. Validation Casting Experiments

An emission validation experiment was designed to compare the analytically measured emission compounds discussed in Section 2 to an actual casting situation. In order to closely represent the analytically measured conditions, the casting and mold design strived for nearly complete combustion of the binder during a one-hour time frame. A simple rectangular casting geometry was chosen to increase the surface area exposed to heat transfer and the volume sufficient large to perform a preliminarily validation of the one-dimensional sand simulation discussed in Section 4.1.

7.1 Validation Methodology and Results

At the University of Northern Iowa Metal Casting Center, a 12" x 8" x 2" rectangular class 30 gray iron casting was poured into a 1.5% phenolic urethane DMEA cured mold. The mold wall thickness surrounding all sides of the casting was 2" in thickness. Prior simulation with a pouring temperature of approximately 2550^{o}F indicated the selected wall thickness would raise the outside mold temperature to approximately 500^{o}F, adequate temperature to decompose a significant portion of the binder into the desired HAP and VOC compounds investigated in the study. A steel sampling port approximately 2" in diameter was position along the longitudinal and lateral centerline of the casting. Copper tubing connected the sampling port to a 6L emission collection canister. Periodically, the copper tubing was heated during sampling to evaporate any condensable compounds collecting inside the tubing. Connected to the canister, a flow controller regulated the sampling flow at 167 mL/min to give a total sampling time of 30 minutes. Two 30-minute emission-sampling segments were conducted for a casting experiment. A total of two casting experiments were conducted.

After emission sampling was conducted, the canisters were sent to reputable environmental emission vendor for GC-MS analysis. EPA Modified TO-15 was specified as the methodology for determining the HAP's and VOC's emitted during the casting experiments. ASTM D-1946 was specified as the analysis technique for carbon monoxide and carbon dioxide determination. All analysis was certified by laboratory.

Table 2 shows the measured HAP's and VOC's corresponding to the 12 identified emission species provide in Table 1. Of the 12 compounds, only hexane, benzene, toluene, xylene (m,p-xylene and o-xylene combined), carbon monoxide, and carbon dioxide was identified by laboratory analysis. The laboratory did not report phenol because EPA TO-15 testing methodology does not accurately quantify this particular chemical species. In addition, methyl oleate and cresols are not considered as hazardous air pollutants and was not tested. Naphthalene was not measured since this is compound is not specified by the Modified TO-15 methodology. Other emission compounds identified during the casting experiment were chloromethane, 1,3-butadiene, ethanol, acetone, 2-butanone, tetrahydrofuran, chlorobenzene, methyl chloride, heptane, ethyl benzene, styrene, propylbenzene, 4-ethyltoluene, 1,3,5-trimethylbenzene, and 1,2,4-trimethylbenzene. These compounds were not reported since they were not originally selected in the initial data collection reported in Section 2.

Table 2 indicated a significant portion of the total emitted decomposition products of phenolic urethane was benzene. Toluene and xylene were emitted in appreciable quantity though not at the substantial level of benzene. These three emission compounds represented the top three species measured in the casting experiments and represented 89% of the emission mass based on the Modified TO-15 analysis methodology. Comparing the analytical data measured in Section 2 to the casting experiment, a significant deviation was observed from the expected results to the actual casting results.

Table 3 shows the ratio of emission species measured by analytical techniques and emitted ratio of the validation casting experiment. Comparison of the benzene to hexane ratio indicates a significantly large emission quantity of benzene than measured by analytical techniques. Higher benzene production was also confirmed when the benzene to toluene and benzene to xylene ratio is calculated. In the validation experiment, only the toluene to xylene emission ratio showed some binder degradation correlation.

7.2 Model Deviation from Casting Experiment

The casting validation experiments measured a significantly higher benzene emission quantity than the measured analytical approach used for the simulation model. Production of toluene during pyrolysis was appreciably greater than the measured analytical method.

The suspected discrepancy between the analytical and validation data can be contributed to the difference in sampling techniques between the test methodologies. In the measured pyrolysis data collected in Section 2, the phenolic urethane sample is slowing heated at a controlled heating rate and decomposition products are continuously removed from the reaction chamber for sampling and identification. Once these emission decomposition products leave

the experimental system, they are no longer available for further decomposition nor will they influence other chemical reaction during subsequent heating.

In an actual casting situation, the decomposition products such as benzene derivatives as xylene, phenol, toluene, and naphthalene remain in the mold and, if the thermal gradient is greater than the condensation wave front prorogating through the mold, decompose into basic benzene molecules. It was shown in figure 7 that the 11-pyrolysis products investigated constituted roughly 20% of the total pyrolysis products. Casting experiments indicated these 11 species contributed to over 90% of the total pyrolysis products. In addition, analytical data collection indicated a carbon monoxide and carbon dioxide level of 2.2 wt% and 8.3 wt%, respectively. Casting experiments showed a carbon monoxide and carbon dioxide level of 4.6 wt% and 5.3 wt%, respectively. These results clearly show other secondary decomposition reactions are occurring inside the mold and the mold atmosphere is establishing equilibrium

7.3 Casting Verification Conclusions/Recommendations

The validation experiment demonstrated complex chemical reactions are occurring inside the phenolic urethane mold that needs to be considered in the simulation model. The research work has revealed the primary reaction mechanism and subsequent emitted compounds of the initial decomposition of phenolic urethane. Secondary reactions promoting chemical equilibrium with the mold atmosphere need to be considered in the model to account for chemical equilibrium and rapid decomposition of the binder and condensation zone. Extensive and detailed analysis of the decomposition and equilibrium reaction of phenolic urethane would require substantial investment, though the simulation benefits would permit casting designers and the foundry industry to solve mold related defects while monitoring environmental emissions of the casting design.

8. References

[1] MAGMASOFT®, MAGMA GmbH, 52072 Aachen, Germany.

[2] M.D. McKinley, C.A. Lytle and W. Bertsch, "Pyrolysis of Core Resins Used in Metalcasting," *AFS Trans.*, 99-41, pp. 407-412.

[3] Y. Wang, F.S. Cannon, M. Salama, D.A. Fonseca and S. Giese (2009), "Characterization of Pyrolysis Products from a Biodiesel Phenolic Urethane Binder," *Environ. Sci. Technol.*, vol. 43(5), pp. 1559-1564.

9. Tables and Figures

Table 1. Total amounts of pyrolysis products captured during TGA pyrolysis of the first sample from 20°C – 900°C at 10°C/min.

Greenhouse Gases	**(mg/g binder)**
CH_4	18.64
CO	22.00
CO_2	82.90
Representative HAPs	**(mg/g binder)**
hexane	0.2690
benzene	1.2579
toluene	2.0088
xylene	1.1174
phenol	3.2202
cresols	2.3101
Other Emissions	**(mg/g binder)**
methyl-naphthalene	1.4491
methyl oleate	9.0004

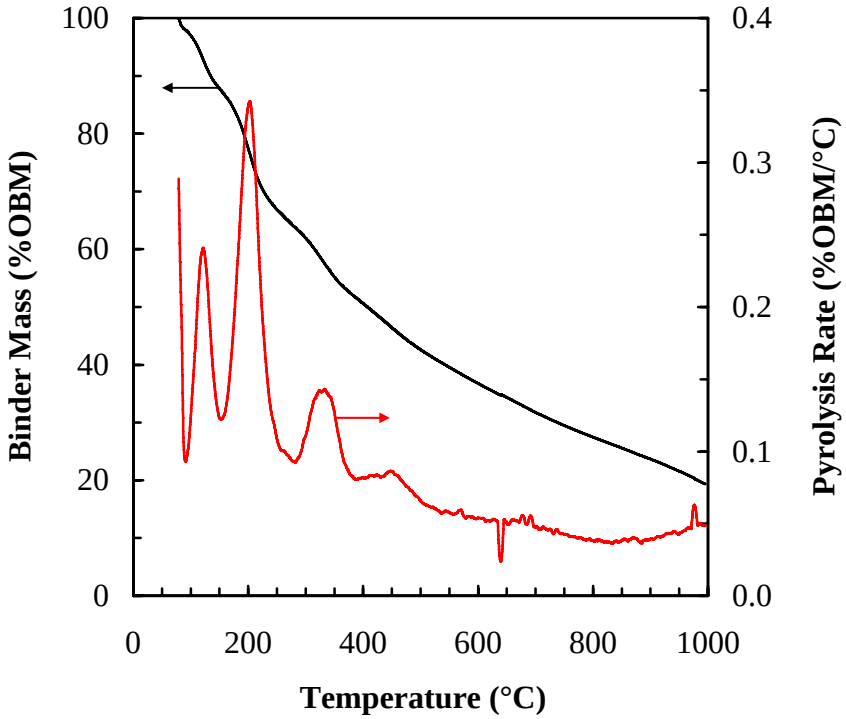


Figure 1. Total binder mass and pyrolysis rate of the second sample as functions of temperature. Values given as a percent of the original binder mass (%OBM).

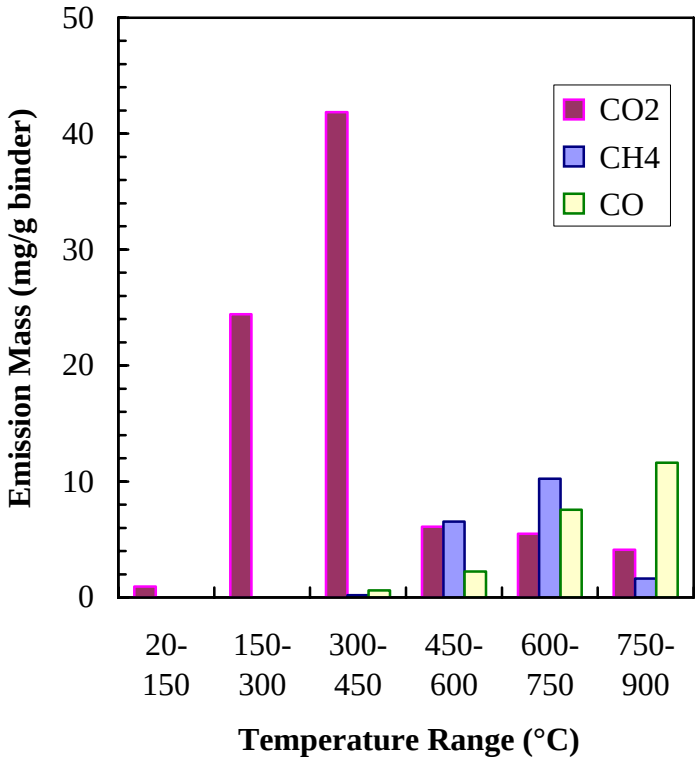


Figure 2. Captured greenhouse gas pyrolysis products from the first sample as a function of temperature range.

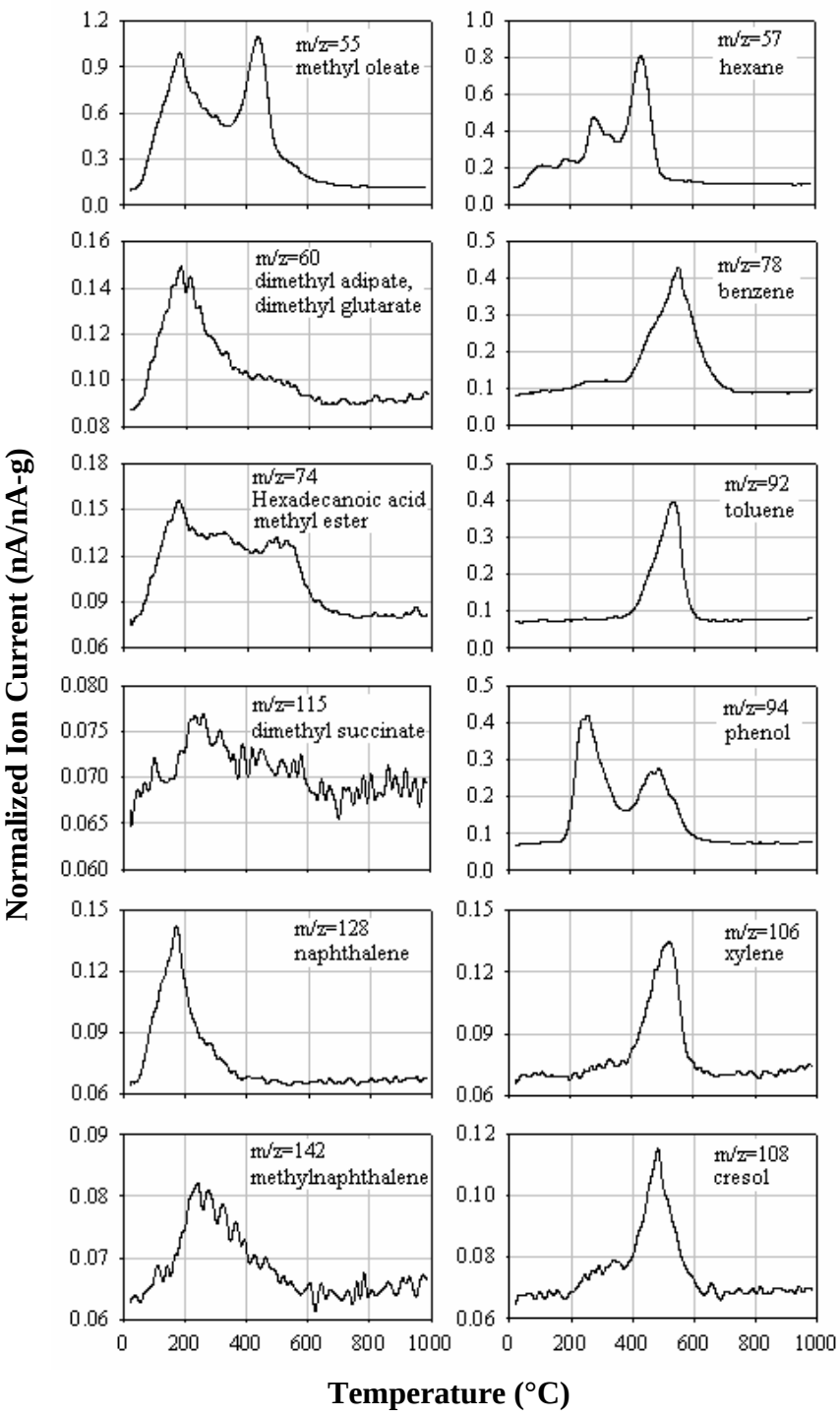


Figure 3. Kinetic measurements of individual gaseous species from pyrolysis of the second sample.

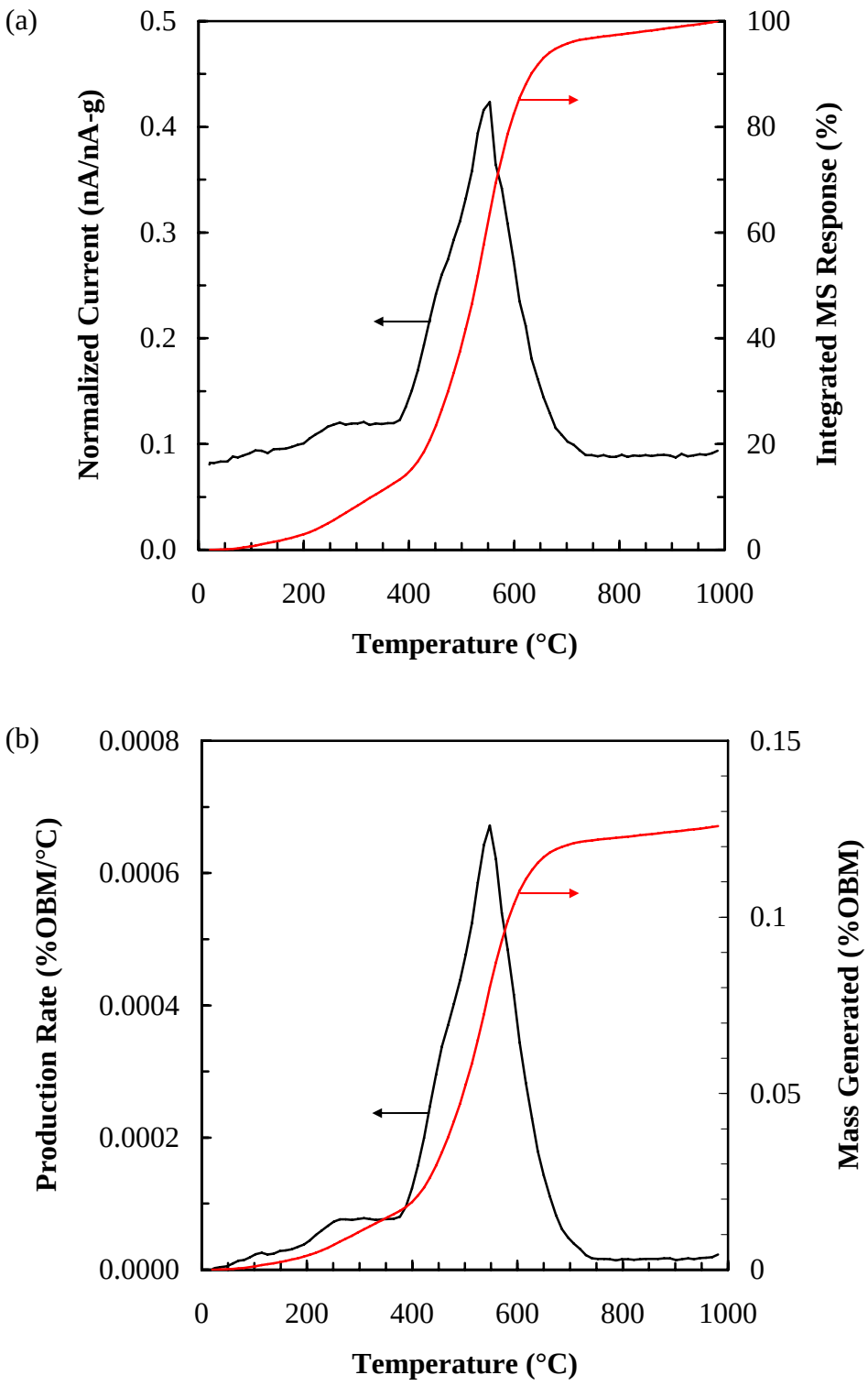


Figure 4. (a) Mass spectrometer (MS) data for benzene, given as normalized current, and the integral of the area under the normalized current curve; (b) Production rate of benzene and total mass of benzene generated, given as a mass fraction.

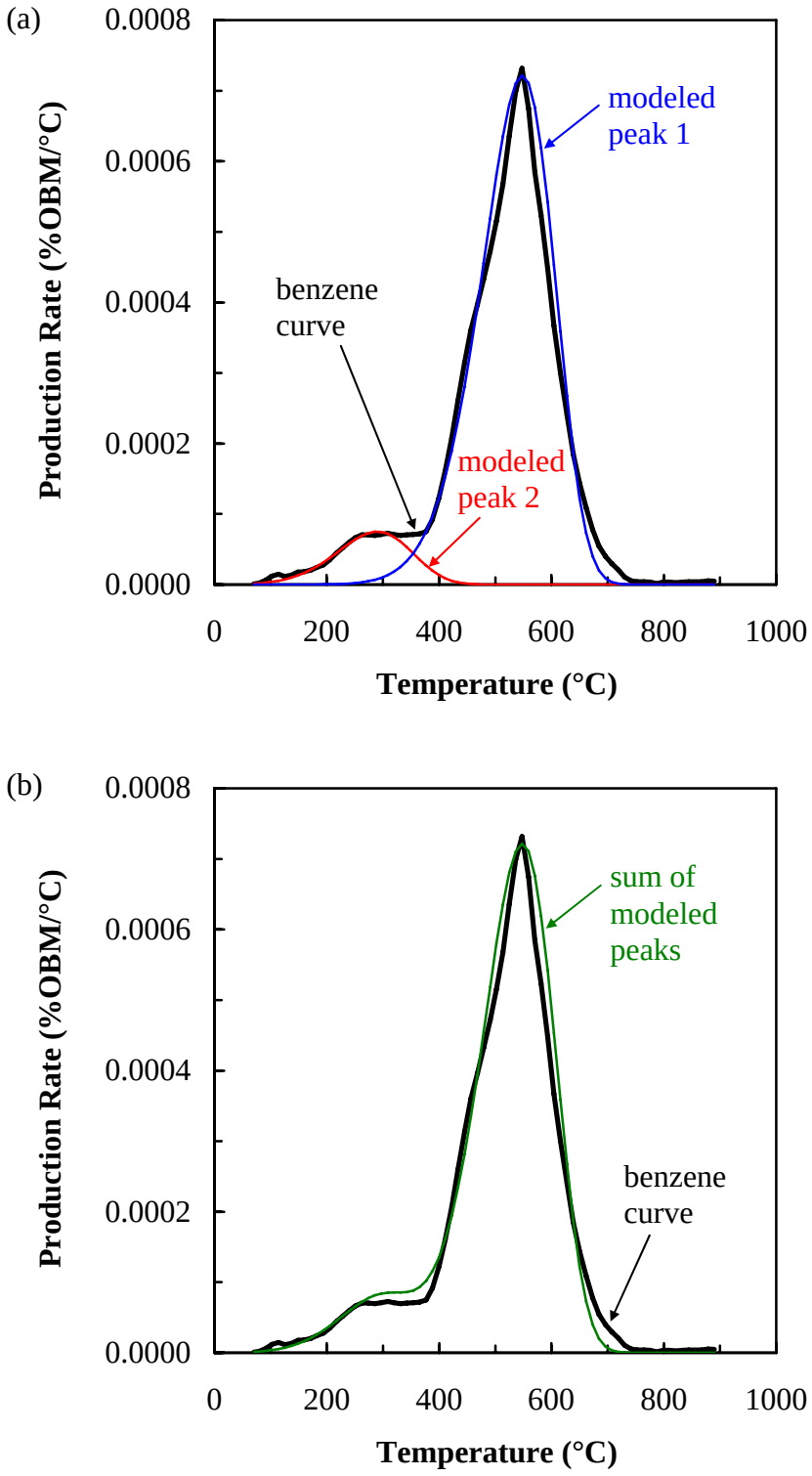


Figure 5. (a) Two model peaks fit to peaks in benzene production rate data; and (b) sum of model peaks, compared to benzene production rate curve.

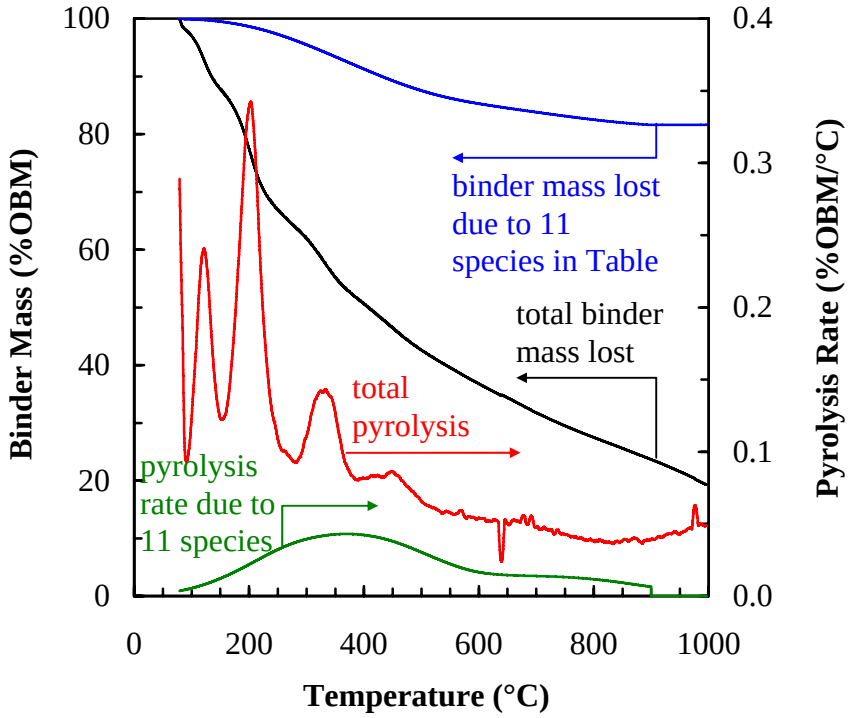


Figure 6. Comparison of total binder mass lost and mass lost due to the 11 species listed in Table 1, as well as a comparison of the corresponding pyrolysis rates.

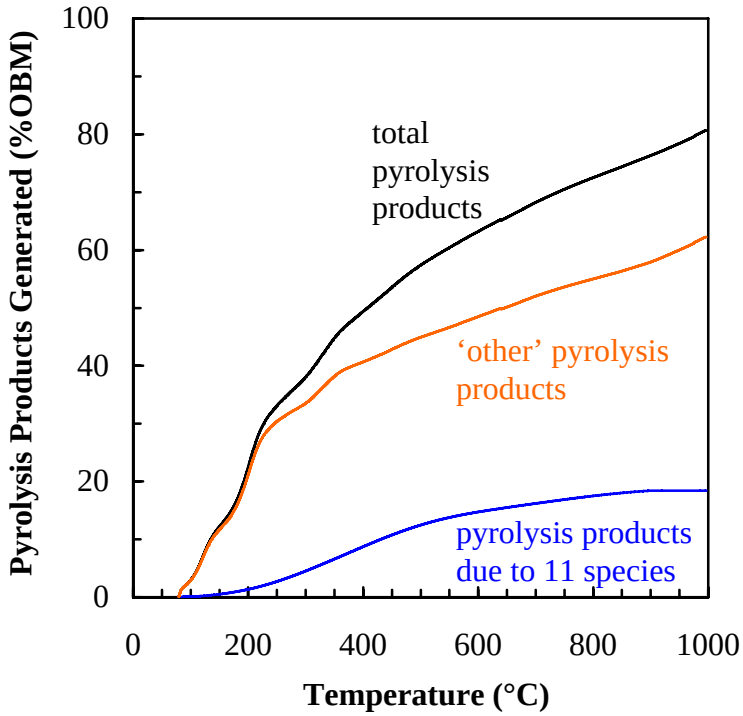


Figure 7. Total pyrolysis products generated, pyrolysis products generated due to the 11 species in Table 1, and the 'other' pyrolysis products generated.

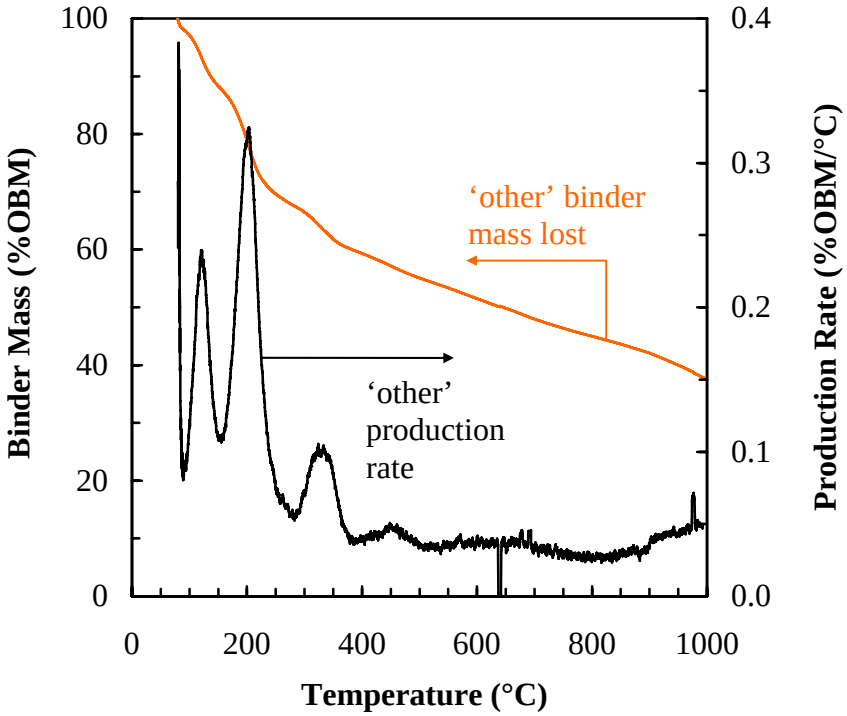


Figure 8. Binder mass lost due to pyrolysis products not listed in Table 1, along with the production rate of these 'other' pyrolysis products.

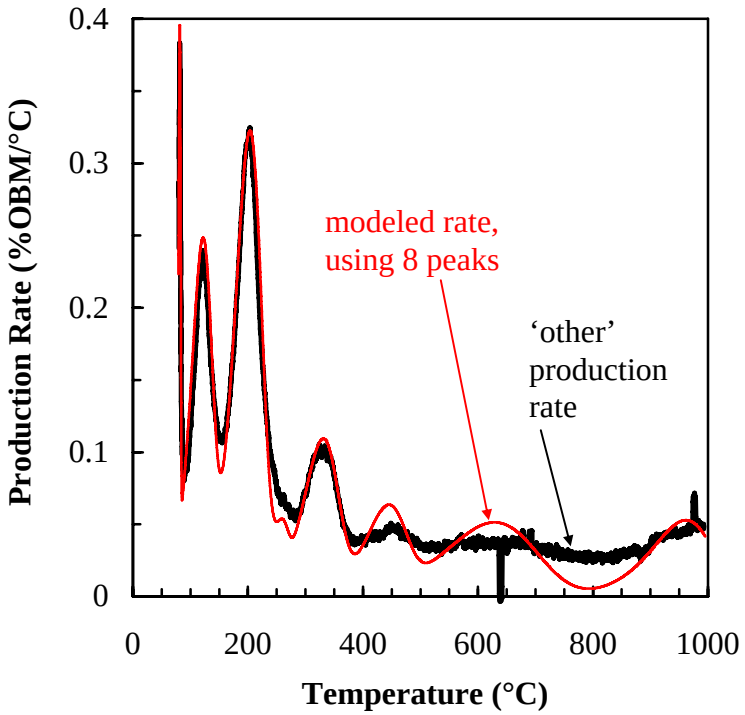


Figure 9. Production rate of 'other' pyrolysis products, along with modeled production rate.

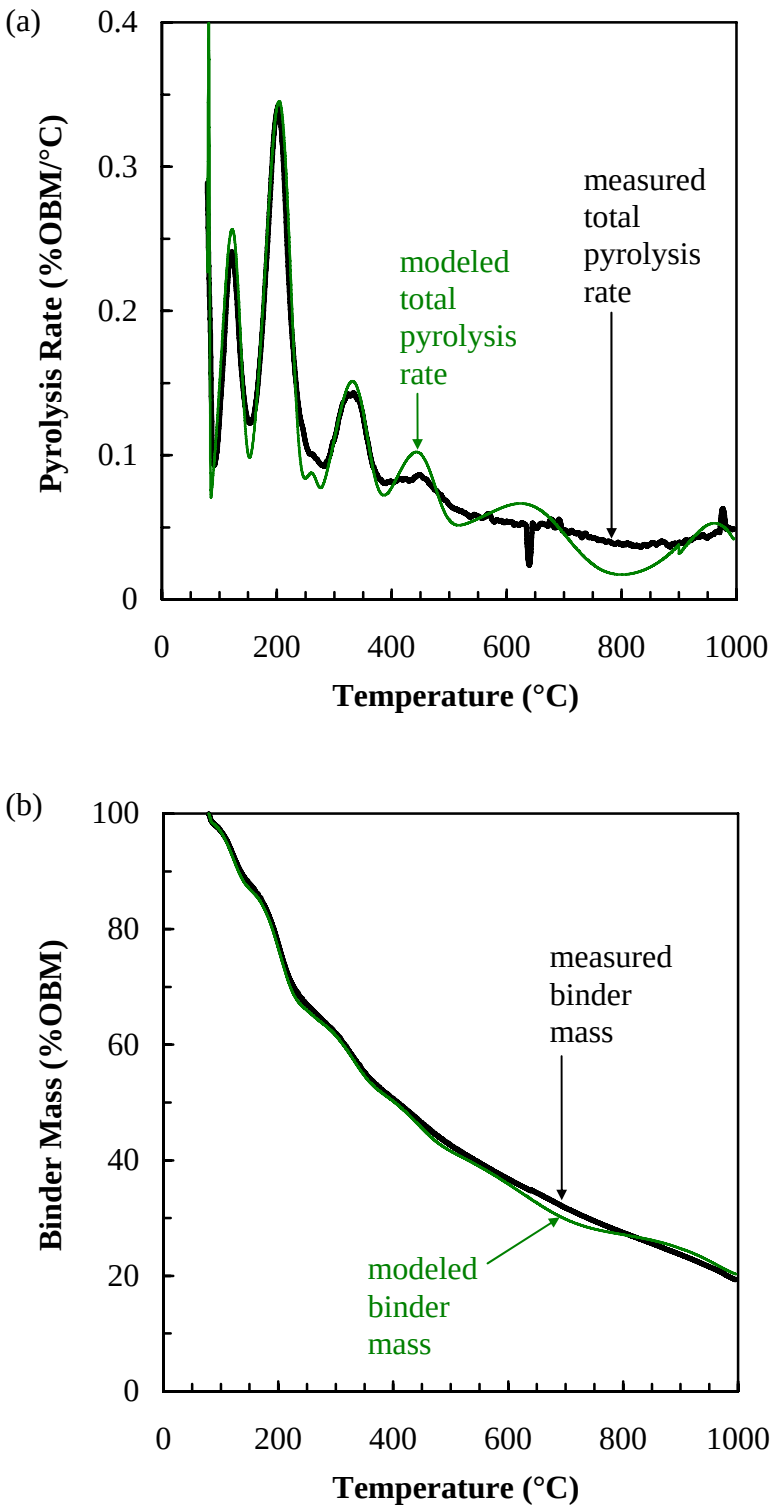


Figure 10. Comparison between (a) measured and modeled total pyrolysis rates; and (b) measured and modeled binder mass, as functions of temperature.

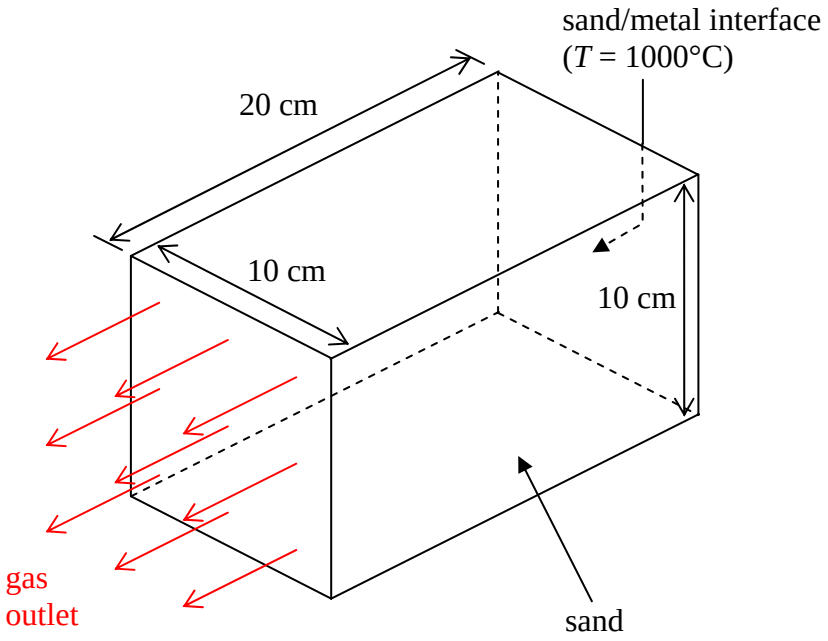


Figure 11. Schematic of domain for 1-D example.

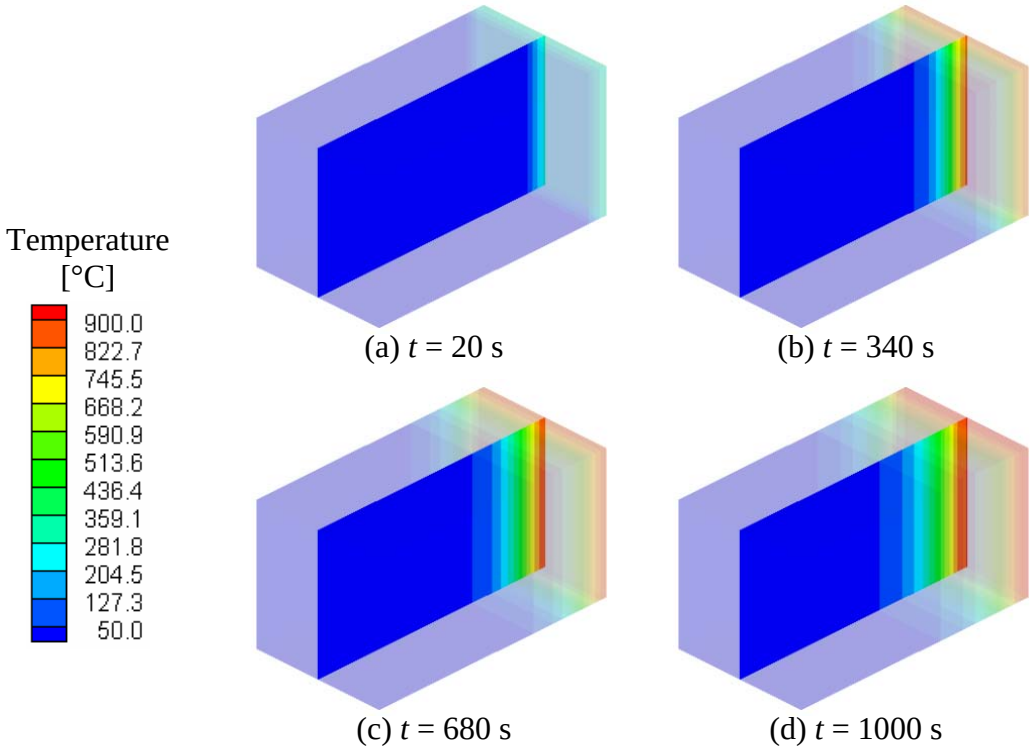


Figure 12. Temperature profiles at various times during the simulation.

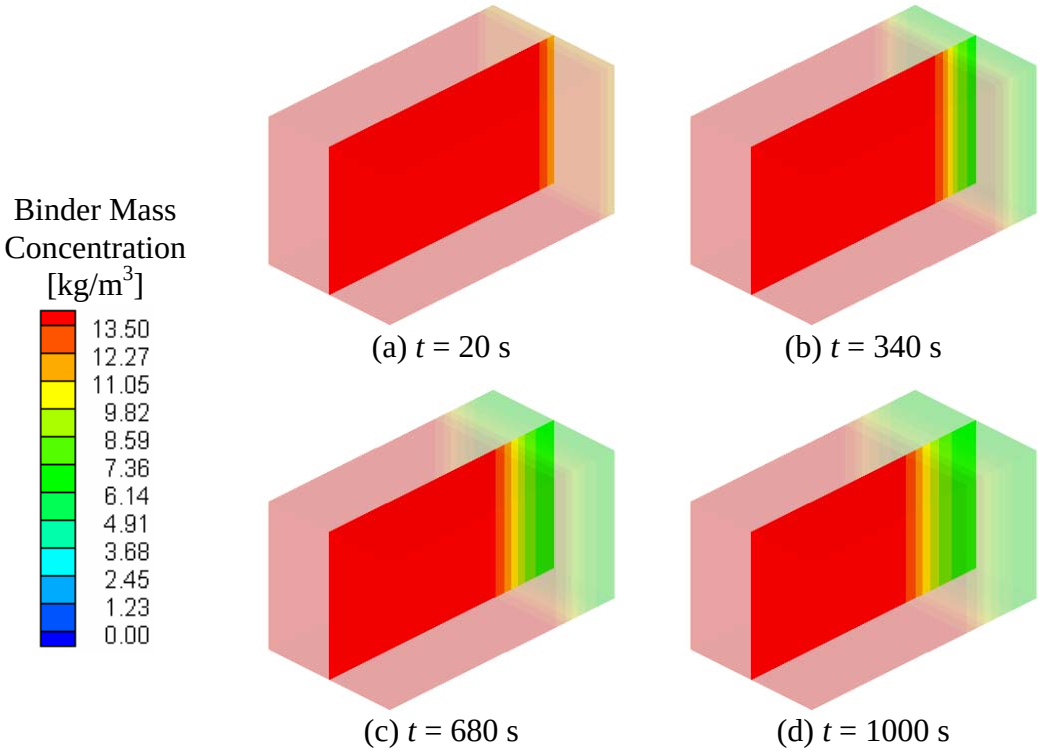


Figure 13. Binder mass concentration profiles at various times during the simulation.

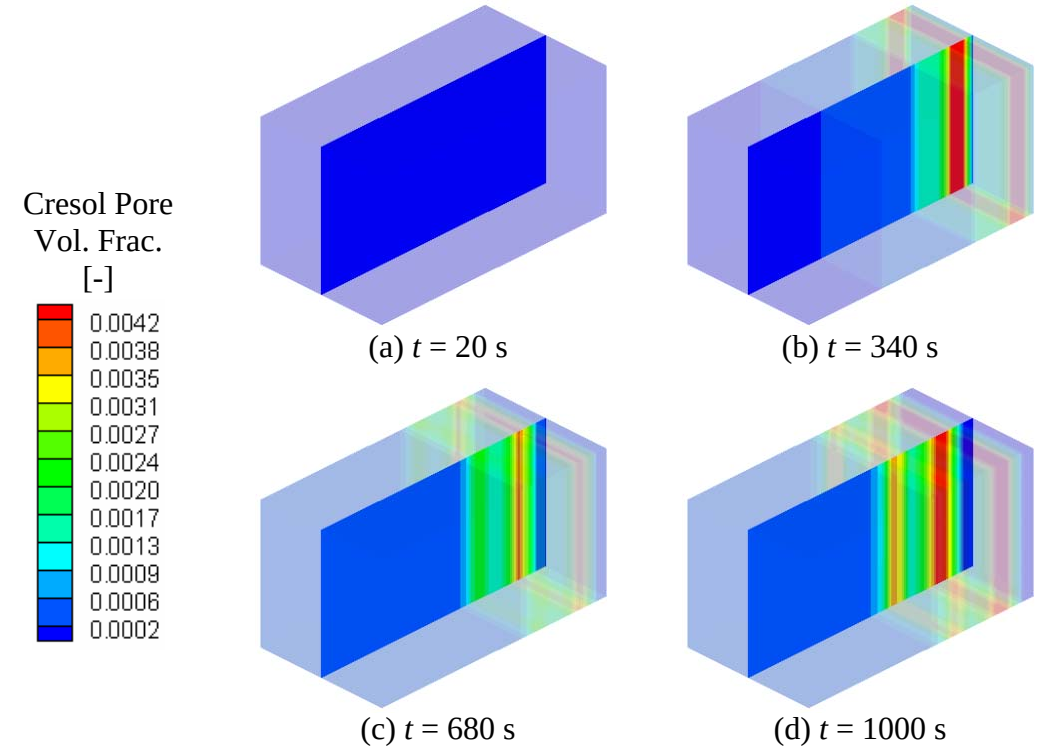


Figure 14. Cresol pore volume fraction profiles at various times during the simulation.

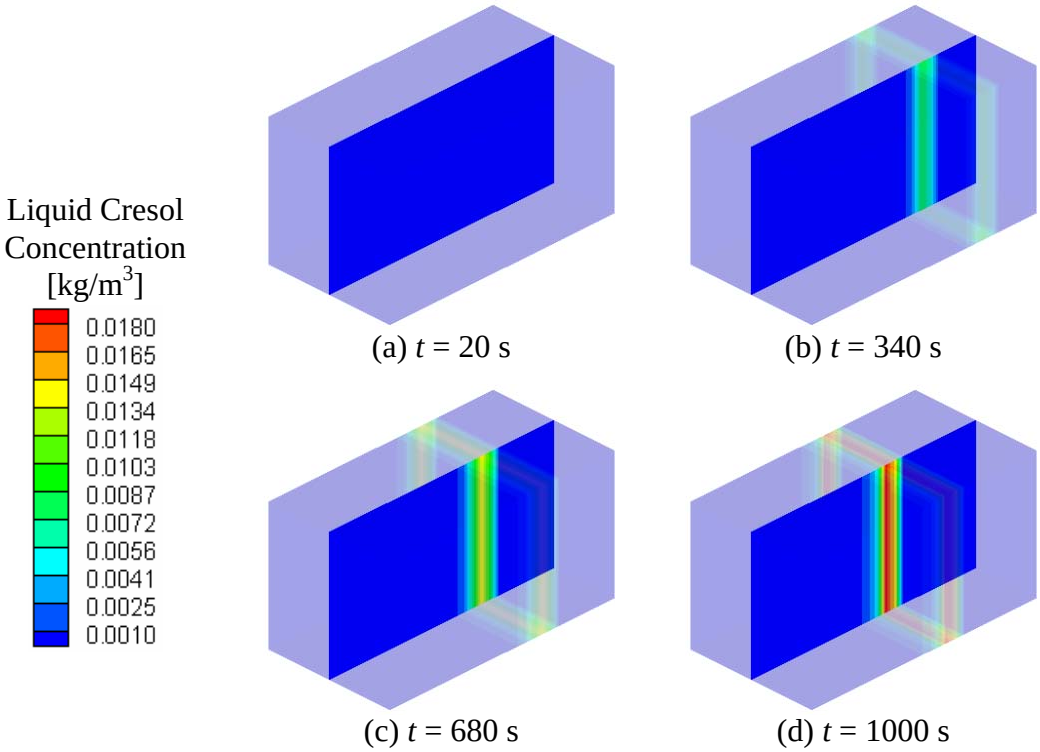


Figure 15. Liquid cresol concentration profiles at various times during the simulation.

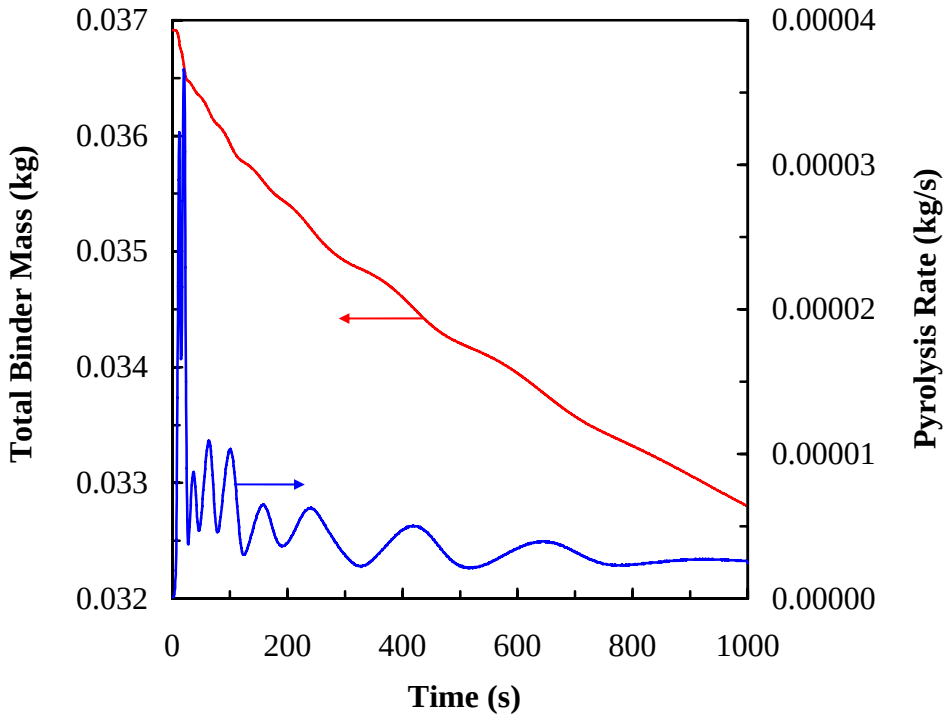


Figure 16. Binder mass and pyrolysis rate as a function of time for sand sample.

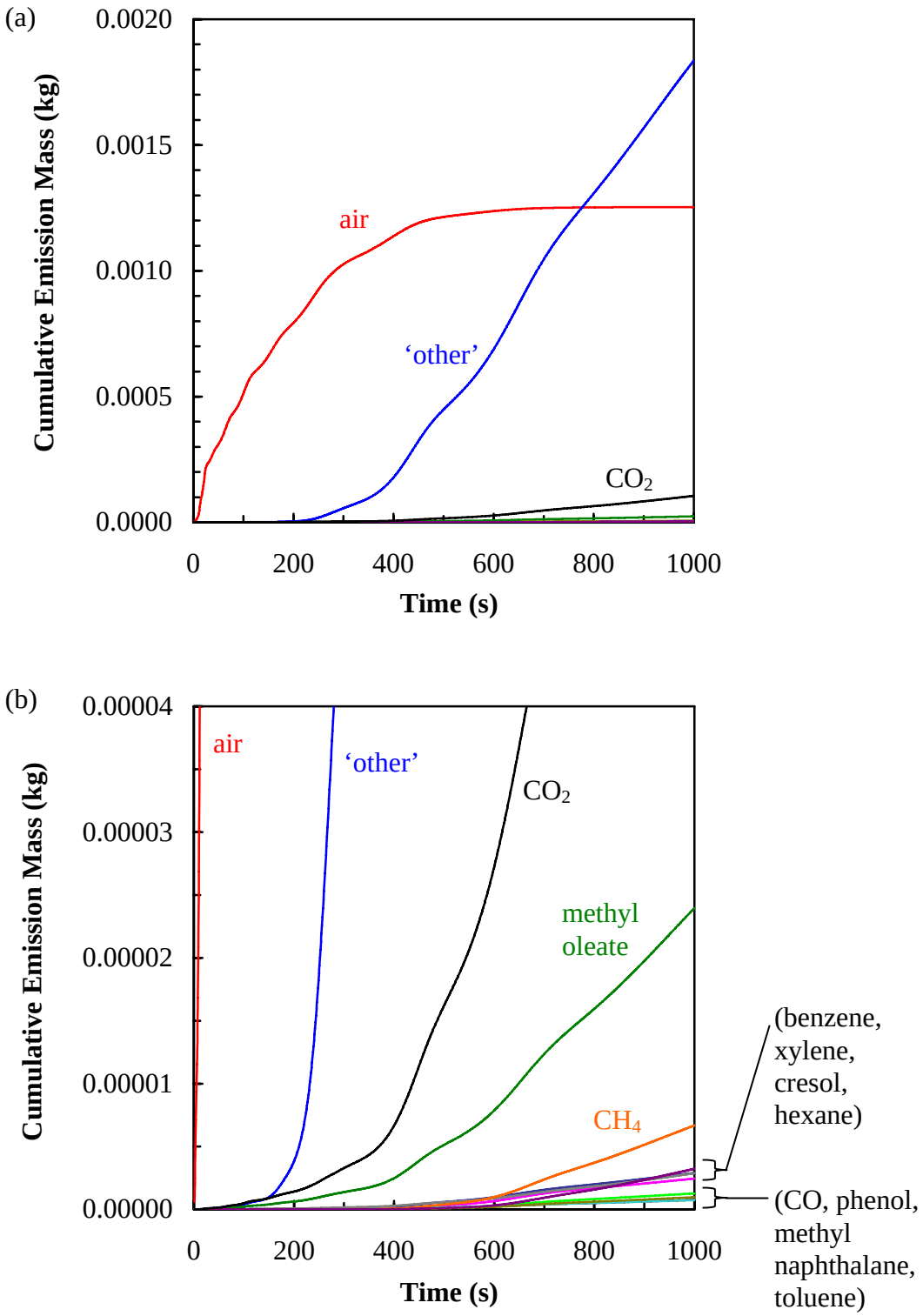


Figure 17. Cumulative species emissions that reach the outlet as a function of time: (a) mass scale showing largest components; and (b) mass scale showing smaller components.

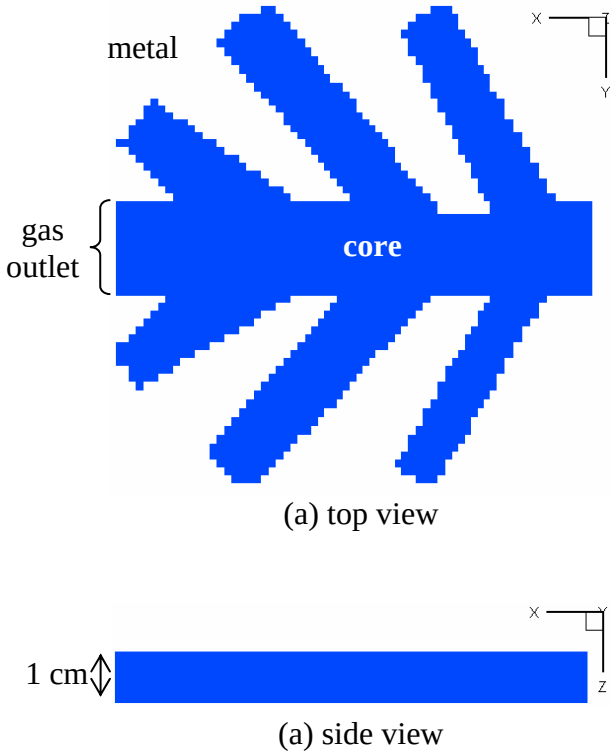


Figure 18. Schematics of tree core: (a) top view; and (b) side view.

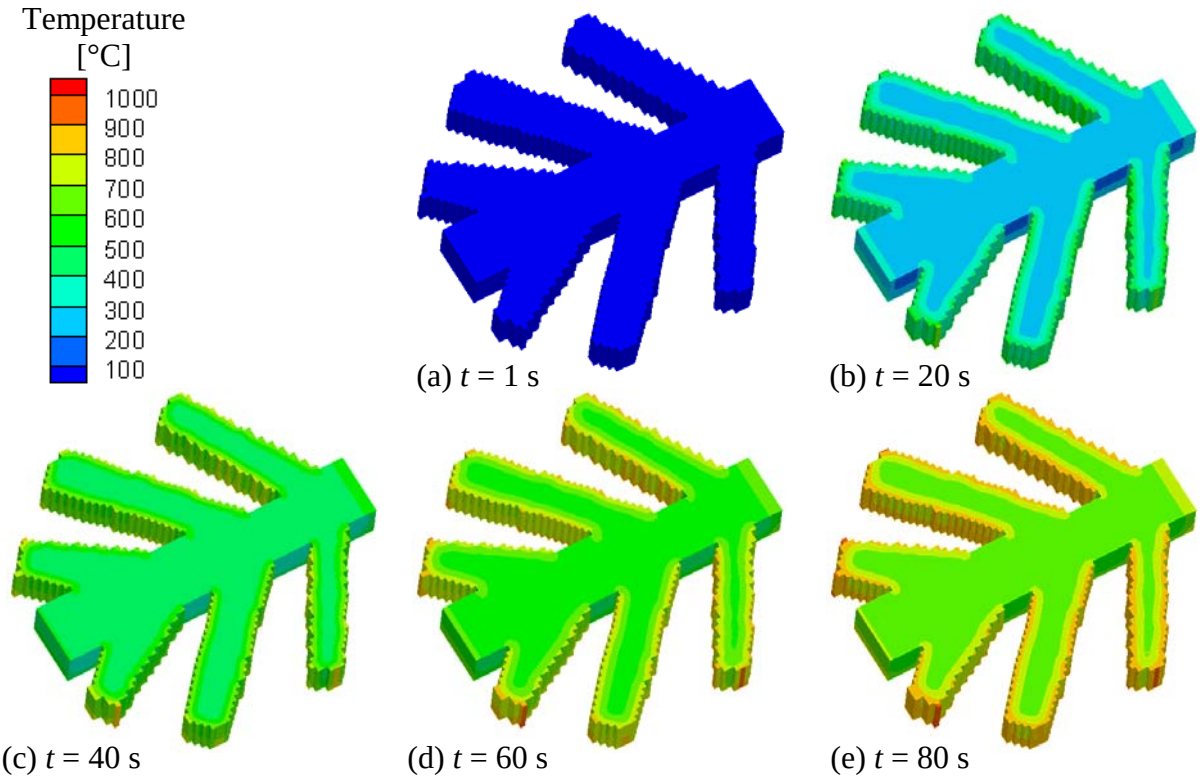


Figure 19. Tree core temperature profiles at various times during the simulation.

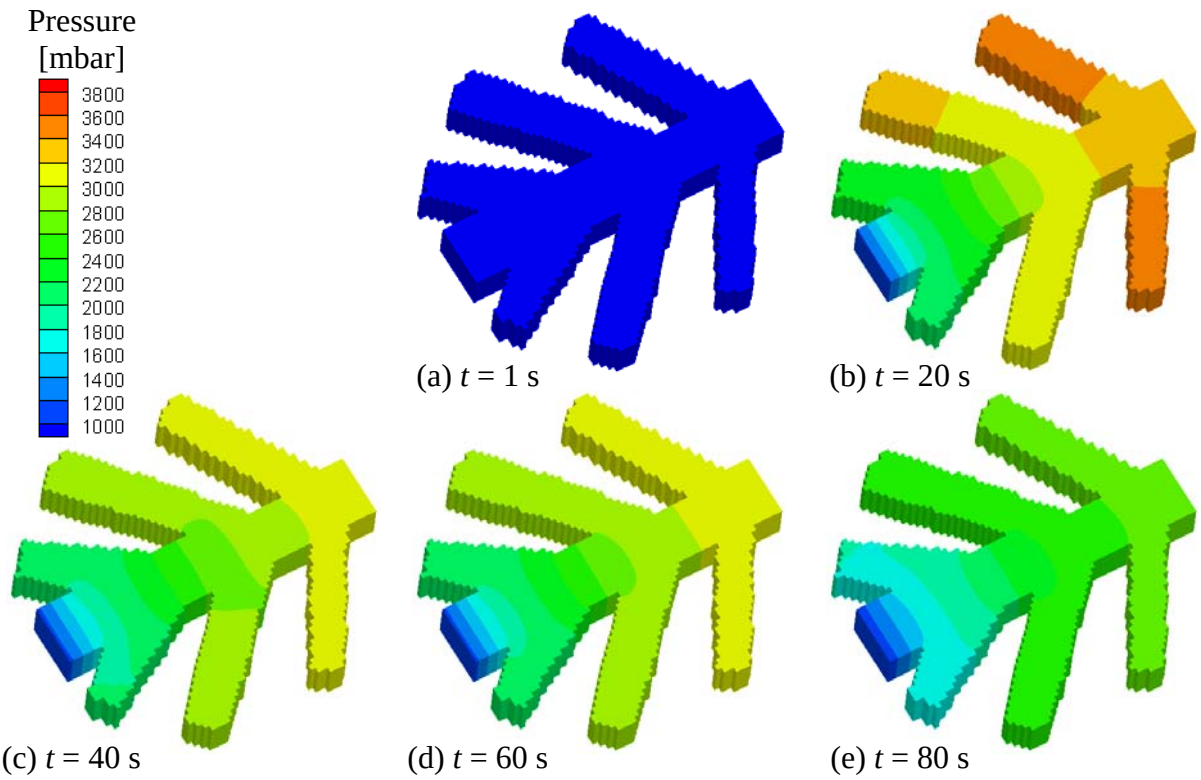


Figure 20. Tree core pressure profiles at various times during the simulation.

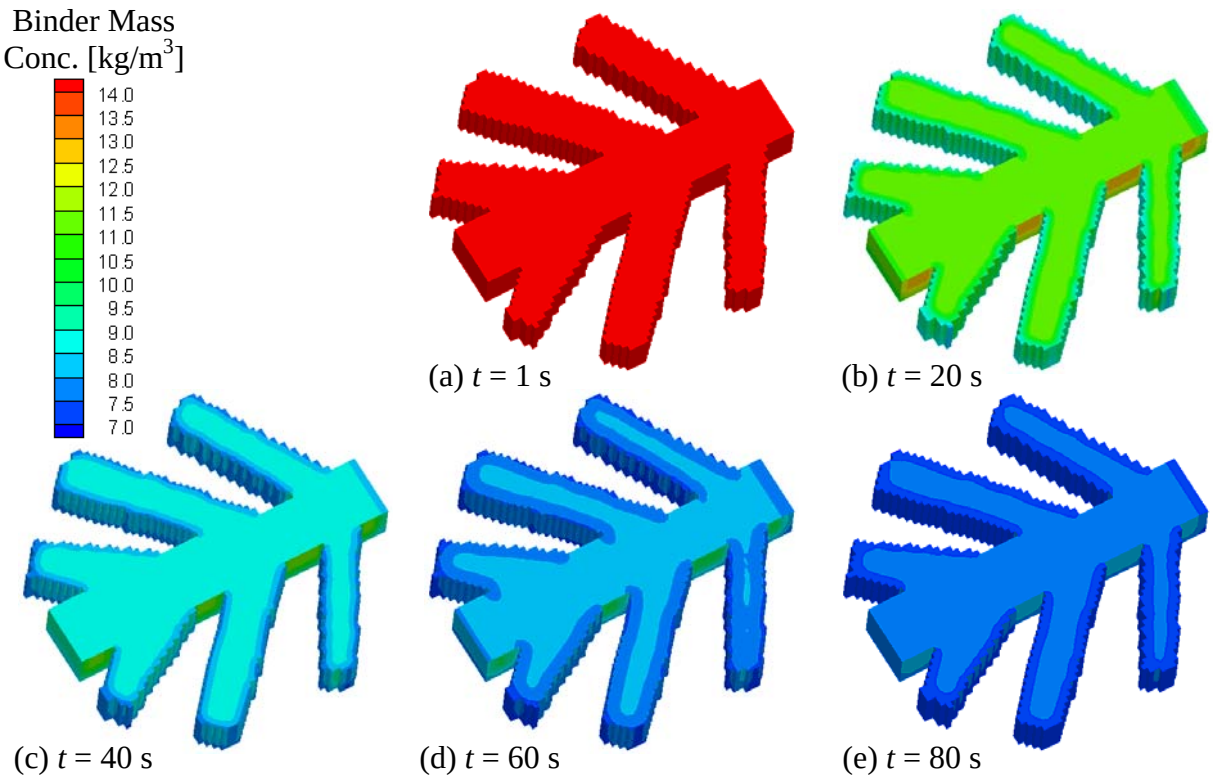


Figure 21. Tree core binder mass concentration profiles at various times during the simulation.

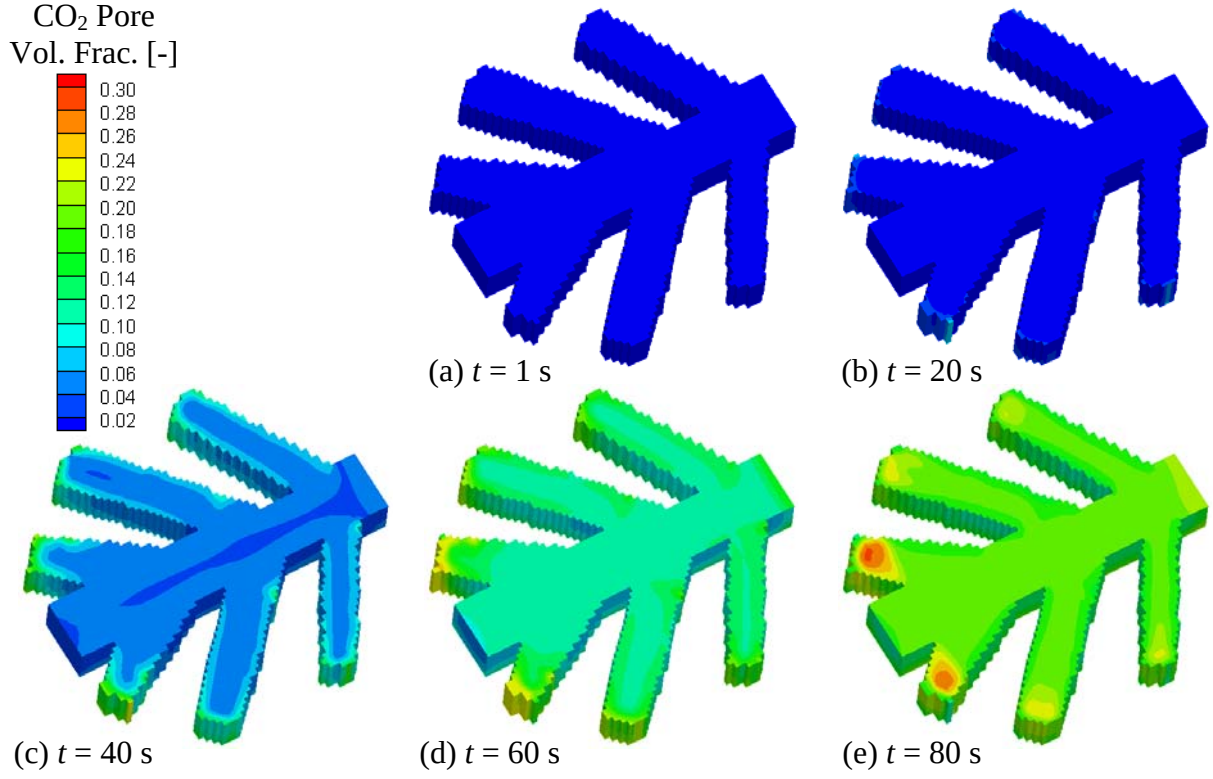


Figure 22. Tree core pressure profiles at various times during the simulation.

Table 2. Emission Production of Model Validation Experiments

	Casting 1			Casting 2		
	1st 30 minutes mg/m^3	2nd 30 minutes mg/m^3	Total Emission mg/m^3	1st 30 minutes mg/m^3	2nd 30 minutes mg/m^3	Total Emission mg/m^3
Hexane	*38*	*34*	72	*43*	*19*	62
Benzene	*6000*	*520*	6520	*7100*	*180*	7280
Toluene	*740*	*160*	900	*900*	*36*	936
Xylene	*199*	*30.4*	229.4	*256*	*11.5*	267.5

Table 3. Comparison of Ratio of HAP's produced during Validation Casting Experiment and Analytical Measurement.

Emission Ratio	Analytical	Casting 1	Casting 2
Benzene/Hexane	4.24	90.6	117.4
Toluene/Xylene	1.80	3.92	3.50
Toluene /Hexane	6.79	12.5	15.1
Xylene/Hexane	3.78	3.19	4.31
Benzene/Toluene	0.63	7.24	7.78
Benzene/Xylene	1.13	28.4	27.2